© 2020. Published by The Company of Biologists Ltd | Journal of Cell Science (2020) 133, jcs240200. doi:10.1242/jcs.240200

RESEARCH ARTICLE

SNAP29 mediates the assembly of histidine-induced CTP synthase filaments in proximity to the cytokeratin network

Archan Chakraborty[1], Wei-Cheng Lin[2,3], Yu-Tsun Lin[2], Kuang-Jing Huang[3], Pei-Yu Wang[2], Ian Yi-Feng Chang[3,4], Hsiang-lu Wang[4], Kung-Ting Ma[5], Chun-Yen Wang[5], Xuan-Rong Huang[5], Yen-Hsien Lee[2], Bi-Chang Chen[6], Ya-Ju Hsieh[3], Kun-Yi Chien[2,7], Tzu-Yang Lin[8], Ji-Long Liu[9,10], Li-Ying Sung[11,12], Jau-Song Yu[1,2,3,13], Yu-Sun Chang[1,3] and Li-Mei Pai[1,2,3,13,*]

ABSTRACT

Under metabolic stress, cellular components can assemble into distinct membraneless organelles for adaptation. One such example is cytidine 5′-triphosphate synthase (CTPS, for which there are CTPS1 and CTPS2 forms in mammals), which forms filamentous structures under glutamine deprivation. We have previously demonstrated that histidine (His)-mediated methylation regulates the formation of CTPS filaments to suppress enzymatic activity and preserve the CTPS protein under glutamine deprivation, which promotes cancer cell growth after stress alleviation. However, it remains unclear where and how these enigmatic structures are assembled. Using CTPS–APEX2-mediated *in vivo* proximity labeling, we found that synaptosome-associated protein 29 (SNAP29) regulates the spatiotemporal filament assembly of CTPS along the cytokeratin network in a keratin 8 (KRT8)-dependent manner. Knockdown of SNAP29 interfered with assembly and relaxed the filament-induced suppression of CTPS enzymatic activity. Furthermore, APEX2 proximity labeling of keratin 18 (KRT18) revealed a spatiotemporal association of SNAP29 with cytokeratin in response to stress. Super-resolution imaging suggests that during CTPS filament formation, SNAP29 interacts with CTPS along the cytokeratin network. This study links the cytokeratin network to the regulation of metabolism by compartmentalization of metabolic enzymes during nutrient deprivation.

KEY WORDS: CTPS filaments, Intermediate filaments, SNAP29, Histidine

[1]Graduate Institute of Biomedical Sciences, College of Medicine, Chang Gung University, Taoyuan 33302, Taiwan. [2]Department of Biochemistry and Molecular Biology, College of Medicine, Chang Gung University, Taoyuan 33302, Taiwan. [3]Molecular Medicine Research Center, Chang Gung University, Taoyuan 33302, Taiwan. [4]Bioinformatics Core Laboratory, Chang Gung University, Taoyuan 33302, Taiwan. [5]Department of Biomedical Sciences, College of Medicine, Chang Gung University, Taoyuan 33302, Taiwan. [6]Research Center for Applied Sciences, Academia Sinica, Taipei 11529, Taiwan. [7]Clinical Proteomics Core laboratory, Chang Gung Memorial Hospital, Linkou, Taiwan. [8]Institute of Cellular and Organismic Biology, Academia Sinica, Taipei 11529, Taiwan. [9]Department of Physiology, Anatomy and Genetics, University of Oxford, Oxford OX1 3PT, UK. [10]School of Life Science and Technology, ShanghaiTech University, Shanghai 201210, China. [11]Agricultural Biotechnology Research Center, Academia Sinica, Taipei 11529, Taiwan. [12]Institute of Biotechnology, National Taiwan University, Taipei 106, Taiwan. [13]Liver Research Center, Chang Gung Memorial Hospital, Linkou, Taiwan.

*Author for correspondence (pai@mail.cgu.edu.tw)

A.C., 0000-0001-9985-0547; W.-C.L., 0000-0003-2970-635X; K.-J.H., 0000-0001-8689-7397; P.-Y.W., 0000-0002-4893-190X; I.Y.-F.C., 0000-0001-5840-2051; K.-T.M., 0000-0001-9598-9867; C.-Y.W., 0000-0003-0967-2535; Y.-H.L., 0000-0001-7696-1375; Y.-J.H., 0000-0003-3853-4342; T.-Y.L., 0000-0002-1968-177X; L.-Y.S., 0000-0002-5552-8262; L.-M.P., 0000-0002-1417-6432

Received 7 October 2019; Accepted 6 March 2020

INTRODUCTION

Metabolic pathways are often compartmentalized to enhance specificity and efficiency. Although membrane-bound organelles are the classical compartments for various metabolic processes, membraneless supramolecular assemblies such as stress granules, p-bodies (Anderson and Kedersha, 2008; Buchan, 2014) and purinosomes (An et al., 2008) are often implicated in regulating specific metabolic pathways in response to cellular stress (Mitrea and Kriwacki, 2016). It has been suggested that phase-separation mechanisms are important for the dynamic assembly of these membraneless organelles (Boeynaems et al., 2018; Mitrea and Kriwacki, 2016; Uversky, 2017).

Cytidine 5′-triphosphate synthase (CTPS, for which there are CTPS1 and CTPS2 forms in mammals) is a rate-determining enzyme in the *de novo* synthesis of CTP, which serves as a substrate for the synthesis of structural components of DNA and RNA and is involved in the formation of phospholipids (Ostrander et al., 1998). CTPS compartmentalizes into filamentous structures under various conditions across species (Carcamo et al., 2011; Ingerson-Mahar et al., 2010; Liu, 2010; Noree et al., 2010). However, the cellular locations of these filamentous compartments remain unidentified, while the Golgi, centrosomes, actin, tubulin and vimentin have been examined for their association with CTPS in human cells (Carcamo et al., 2011). In yeast, it has been suggested that CTPS filaments are composed of inactive dimers (Noree et al., 2014), although cryo-electron cryomicroscopy (cryo-EM)-based studies in *E. coli* and humans have shown that tetramers are the units of CTPS filament formation (Barry et al., 2014; Lynch et al., 2017). CTPS in its active homotetramer configuration converts UTP into CTP by adding an amino group from glutamine (Gln) (Endrizzi et al., 2004; Goto et al., 2004; Kursula et al., 2006; Weng and Zalkin, 1987), which serves as a key regulator for the reversible assembly of CTPS filaments (Calise et al., 2014; Pai et al., 2016). In human cancer cells, Gln starvation induces CTPS filaments, which are known as ‘rods and rings’ (RR) structures that also contain inosine monophosphate dehydrogenase 2 (IMPDH2) (Calise et al., 2014; Carcamo et al., 2011; Chen et al., 2011; Gou et al., 2014). RR structures can also be induced by CTPS inhibitors, such as 6-diazo-5-oxo-L-norleucine (DON), azaserine and acivicin (Calise et al., 2014; Carcamo et al., 2011; Chen et al., 2011), which are Gln analogs.

It has been proposed that cytoophidium or CTPS filament formation could be an adaptive mechanism to compromise and regulate cell metabolism (Aughey et al., 2014; Petrovska et al., 2014; Wang et al., 2015). In *Drosophila*, activated Cdc42 kinase (Ack), Casitas B-lineage lymphoma (Cbl) and Myc have been shown to regulate the CTPS filament structure in egg chambers (Aughey et al., 2016; Strochlic et al., 2014; Wang et al., 2015). Given that filament formation of CTPS is dynamic, post

Journal of Cell Science (2020) 133, jcs240200. doi:10.1242/jcs.240200

translational modifications, such as ubiquitination and methylation, are required for CTPS filament formation in human cancer cells (Lin et al., 2018; Pai et al., 2016). In human cancer cells, we previously demonstrated that histidine (His) catabolism contributed to the folate cycle and methyl cycle, which are required for CTPS filament formation under Gln deprivation (Lin et al., 2018). The dynamic behavior of CTPS intrigued us, and hence we sought to investigate how filament assembly happens. Conventional methods like co-immunoprecipitation assays have been challenging for the identification of proteins interacting with CTPS filaments. Therefore, we used APEX2-mediated proximity labeling (Lam et al., 2015; Martell et al., 2012) of CTPS1 to identify proteins that are associated with CTPS1 filaments and/or involved in the process of CTPS1 filament formation.

Here, we demonstrate that in human cancer cells during Gln starvation, CTPS is assembled into filament-like structures along the cytokeratin network. Our findings suggest that disrupting the cytokeratin network or knocking down a specific keratin, KRT8, can affect the CTPS filament formation process. Furthermore, we found a SNARE-binding protein, synaptosome-associated protein 29 (SNAP29), that interacts dynamically with the cytokeratin network, which is involved in CTPS filament formation. In summary, we revealed that cytokeratin is an important compartment for the assembly of metabolic enzymes, such as CTPS and IMPDH, into filamentous structures under Gln starvation stress.

RESULTS

Regulators of CTPS filament formation identified by APEX2 proximity labeling

Our previous study revealed that in Gln- and serum-depleted [G(−)/S(−)] conditional medium, His is essential for CTPS filament formation, and His under Earle's buffered salt solution (EBSS) conditions robustly induced CTPS filaments in a dose-dependent manner in HEp-2 cells, thus providing an excellent tool for investigating the process of CTPS filament formation (Fig. 1A; Fig. S1A,B) (Lin et al., 2018). Therefore, we used APEX2-mediated proximity labeling to identify proteins related to CTPS1 filament formation (Fig. 1B) (Lam et al., 2015; Martell et al., 2012). We exogenously C-terminally tagged CTPS1 with the 28-kDa peroxidase APEX2 and N-terminally with a small 3×FLAG tag. The double-tagged CTPS1 assembled into filaments and dissembled with the addition of Gln; thus, these filaments were phenotypically similar to endogenous CTPS filaments (Fig. S2A,B)

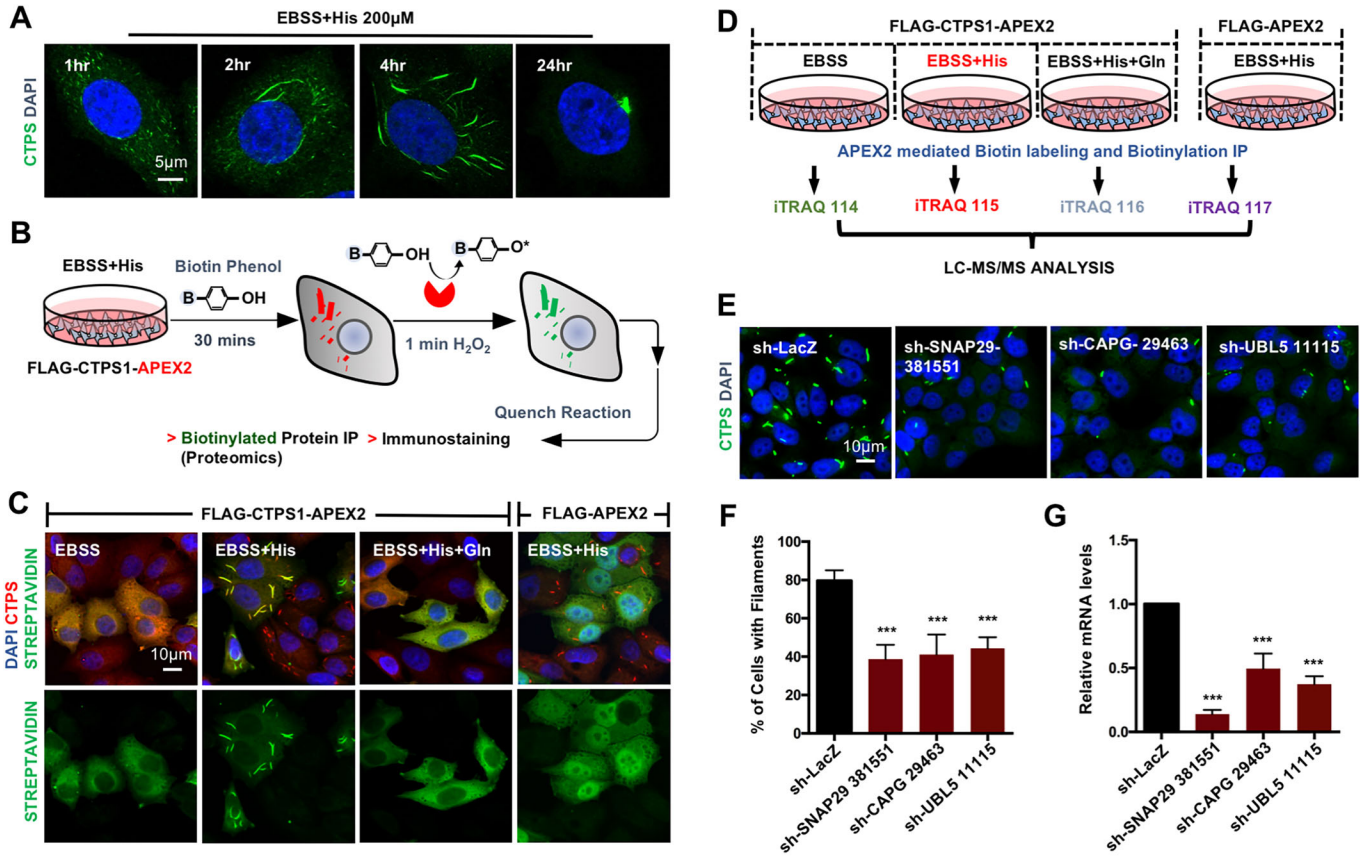

Fig. 1. A screen for CTPS filament-associated proteins. (A) Representative image of CTPS filament assembly at different time points under EBSS+His conditions. HEp-2 cells were immunostained with anti-CTPS (green) antibodies and DAPI (blue). (B) Schematic representation of the strategy used for biotinylation of CTPS1 filaments. IP, immunoprecipitation. (C) Streptavidin staining of HEp-2 cells expressing FLAG–CTPS1–APEX2 in EBSS, EBSS+His, EBSS+His+Gln and FLAG-APEX2 in EBSS+His conditions after 6 h of incubation. Biotinylation signals were detected using streptavidin–Alexa Fluor 488 conjugate (green), CTPS, with anti-CTPS (red) antibodies, and nuclei, with DAPI (blue). (D) Pictorial representation of the strategy used for iTRAQ labeling to identify proteins involved in CTPS1 filament formation. (E,F) shRNA-mediated stable cell knockdown of candidate genes SNAP29, CAPG and UBL5 (sh-SNAP29, sh-CAPG and sh-UBL5), which showed reduced CTPS filament formation in the EBSS+His 50 μM condition at 24 h. The percentage of cells bearing CTPS filaments was calculated for three independent experiments. (G) Relative SNAP29, CAPG and UBL5 mRNA expression was measured by qPCR in sh-SNAP29, sh-CAPG and sh-UBL5 stable knockdown cells, respectively, cultured in DMEM. Results in F and G are mean±s.d. shRNA against LacZ (sh-LacZ) was used as a control. ***P<0.001 (Student's t-test).

Journal of Cell Science (2020) 133, jcs240200. doi:10.1242/jcs.240200

(Calise et al., 2014). As 90% of the cells already induced CTPS filaments within 6 h when treated with 200 µM His in EBSS medium, we chose this condition for proteomic analysis (Fig. S1A,B). FLAG–CTPS1–APEX2 formed filaments within 6 h, and the filaments were also efficiently biotinylated (Fig. 1C). Consistent with this, 15 min of Gln treatment led to the complete disassembly of the FLAG–CTPS1–APEX2 filaments and generated a cytosolic biotin signal (Fig. 1C). Moreover, endogenous CTPS filaments were not biotinylated in cells expressing FLAG–APEX2 alone (Fig. 1C). To detect biotinylated CTPS protein by western blotting, four biological samples [FLAG–CTPS1–APEX2 in EBSS (group 1), EBSS+His (group 2) and EBSS+His+Gln (group 3), and FLAG–APEX2 in EBSS+His (group 4)], were subjected to immunoprecipitation with streptavidin-coated magnetic beads and then probed with anti-CTPS antibody. Exogenous CTPS1 (~100 kDa) was detected in groups 1–3 but not in the control group 4 (Fig. S2C). Furthermore, endogenous CTPS (~70 kDa) was enriched in the EBSS+His group (group 2) (Fig. S2C). These results suggested that APEX2-tagged CTPS1 was assembled with endogenous CTPS into a filamentous structure.

We used isobaric tags for relative and absolute quantification (iTRAQ) followed by two-dimensional liquid chromatography-tandem mass spectrometry (2D LC-MS/MS) (Fig. 1D) (Wiese et al., 2007). FLAG–APEX2 (group 4) served as a non-specific interaction control. Group 2 served as the experimental group, as the presence of FLAG–CTPS1–APEX2 and His together facilitated biotinylation of CTPS filament-interacting proteins. Groups 1 and 3 served as the non-filament and filament-disassembly controls, respectively. Following APEX2 proximity biotinylation and immunoprecipitation, 10% of the immunoprecipitation product from each of the four groups was used to detect the immunoprecipitation efficiency, through silver staining, for quality control (Fig. S2D). The remaining samples were labeled with iTRAQ reagent followed by detection using 2D LC-MS/MS (Fig. 1D). From the iTRAQ analysis, we found 26 shared candidates when comparing the biotinylated filament group 2 to the other three non-biotinylated filament controls (Fig. S2E,F; Table S1). We identified CTPS2, which was previously reported to form filaments in both yeast and humans (Gou et al., 2014; Noree et al., 2010; Shen et al., 2016). Indeed, immunofluorescence staining of FLAG–CTPS2 showed filaments under EBSS+His conditions (Fig. S2G). We then tested the effects of most of the 26 candidate genes on filament formation by performing shRNA-mediated stable cell knockdown. The following three genes showed reduced filaments when incubated with His in the EBSS condition: SNAP29, ubiquitin-like 5 (UBL5) and capping actin protein (CAPG) (Fig. 1E,F). Gene knockdown of these three candidates was also confirmed using quantitative (q)PCR (Fig. 1G).

SNAP29 is required for CTPS filament assembly

We performed 6-plex Tandem Mass Tag (TMT) labeling followed by 2D LC-MS/MS with three repeats of comparison between EBSS+His and EBSS to identify His-induced CTPS filament-interacting proteins (Fig. 2A; Fig. S2H–J and Table S2). We used $P<0.05$ as the initial cutoff and further used mean+2s.d. to select 123 proteins, which included CTPS1, CTPS2 and SNAP29 (Fig. 2A). As SNAP29, a SNARE-binding protein, is known to be involved in multiple protein trafficking processes (Guo et al., 2014; Morelli et al., 2014; Rapaport et al., 2010; Steegmaier et al., 1998), we further studied its involvement in CTPS filament assembly. SNAP29 enrichment during CTPS filament formation was also confirmed by western blot analysis of samples from the CTPS–APEX2-mediated proximity labeling (Fig. S3A). A second set of shRNAs targeting SNAP29 also reduced the proportion of cells with CTPS filaments (Fig. 2B) without affecting CTPS1 protein levels (Fig. 2C). A proximity ligation assay (PLA) confirmed the close proximity of CTPS1 and SNAP29 during filament formation, which yields a signal when two proteins of interest are within a 40-nm distance (Fig. S3B). In our previous study, we found that the *in vivo* enzymatic activity of CTPS was reduced with filament formation induced by His (Lin et al., 2018). However, in SNAP29-knockdown HEp-2 cells, the activity of CTPS was less affected by His addition, which might be due to the reduced filament formation (Fig. 2D; Figs S3C and S2D). Furthermore, the effect of SNAP29 siRNA, which relaxed the suppression of CTPS enzymatic activity, was reversed by overexpression of an siRNA-resistant SNAP29 construct (Fig. S3E,F). Collectively, the formation of CTPS filament mediated by SNAP29 is required to control the enzymatic activity of CTPS for adapting to Gln depletion stress.

We further used electron microscopy (EM) to examine CTPS filaments by anti-Flag gold labeling in HEp-2 cells expressing FLAG–CTPS–APEX2 under His induction, and some of the filament-like structures were labeled with gold particles (Fig. 2Ea–c; Fig. S3Ga). Further attempts to understand the interaction between CTPS and SNAP29 using immunoEM revealed that some SNAP29 signal was detected near the filamentous structures (Fig. 2Ed,e; Fig. S3Gb). Other membranous organelles also showed positive signals for SNAP29 (Fig. 2Ef). Approximately 36% and 40% of gold particles were labeled on filament-like structures for FLAG–CTPS1–APEX2 and FLAG–SNAP29, respectively (Fig. S3H). Even though filament-like structures were distinct under immunoEM, and some of them were positive for CTPS signals, we cannot exclude the possibility of the presence of other polymers in the same area.

CTPS filaments assemble along the cytokeratin network

SNAP29 mutation in humans leads to cerebral dysgenesis, neuropathy, ichthyosis and keratoderma (CEDNIK) syndrome, which is related to the defective transportation of components in keratinocytes during epidermal differentiation (Fuchs-Telem et al., 2011; Sprecher et al., 2005). Intriguingly, we found many keratin proteins were identified in our iTRAQ analysis comparisons between HIS and APEX, HIS and EBSS, and HIS and GLN (Fig. S2F, Table S1). Arguably, keratin proteins are well known contaminants in mass spectrometry. However, Gene Set Enrichment Analysis (GSEA) for proteins identified using a TMT labeling assay also showed enrichment for keratin filament proteins (Fig. S3I, Table S3) (Mootha et al., 2003; Subramanian et al., 2005). Taken together, a pan-cytokeratin antibody was initially used to observe whether CTPS filaments were located along the cytokeratin network in HEp-2 cells. Indeed, we observed CTPS filaments along the cytokeratin track on super-resolution images (Fig. 3A,B; Fig. S4A). Imaging at different time points, CTPS displayed a spatiotemporal association along the cytokeratin network (Fig. 3B). Under G(−)S(−) conditions, CTPS and IMPDH2, an enzyme of the purine biosynthesis pathway, assembled into filamentous structures along the cytokeratin network (Fig. S4B,C). However, it is unclear whether IMPDH2 filament assembly was dependent on CTPS as partial knockdown of CTPS did not affect IMPDH2 filament assembly in glutamine depletion medium (Fig. S4D,E). CTPS filaments were also found on the cytokeratin network in HeLa cells (Fig. S4F). There are more than 50 isomers of keratin that are subdivided into type I (K9–K28, K31–K40) and type II (K1–K8,

Journal of Cell Science (2020) 133, jcs240200. doi:10.1242/jcs.240200

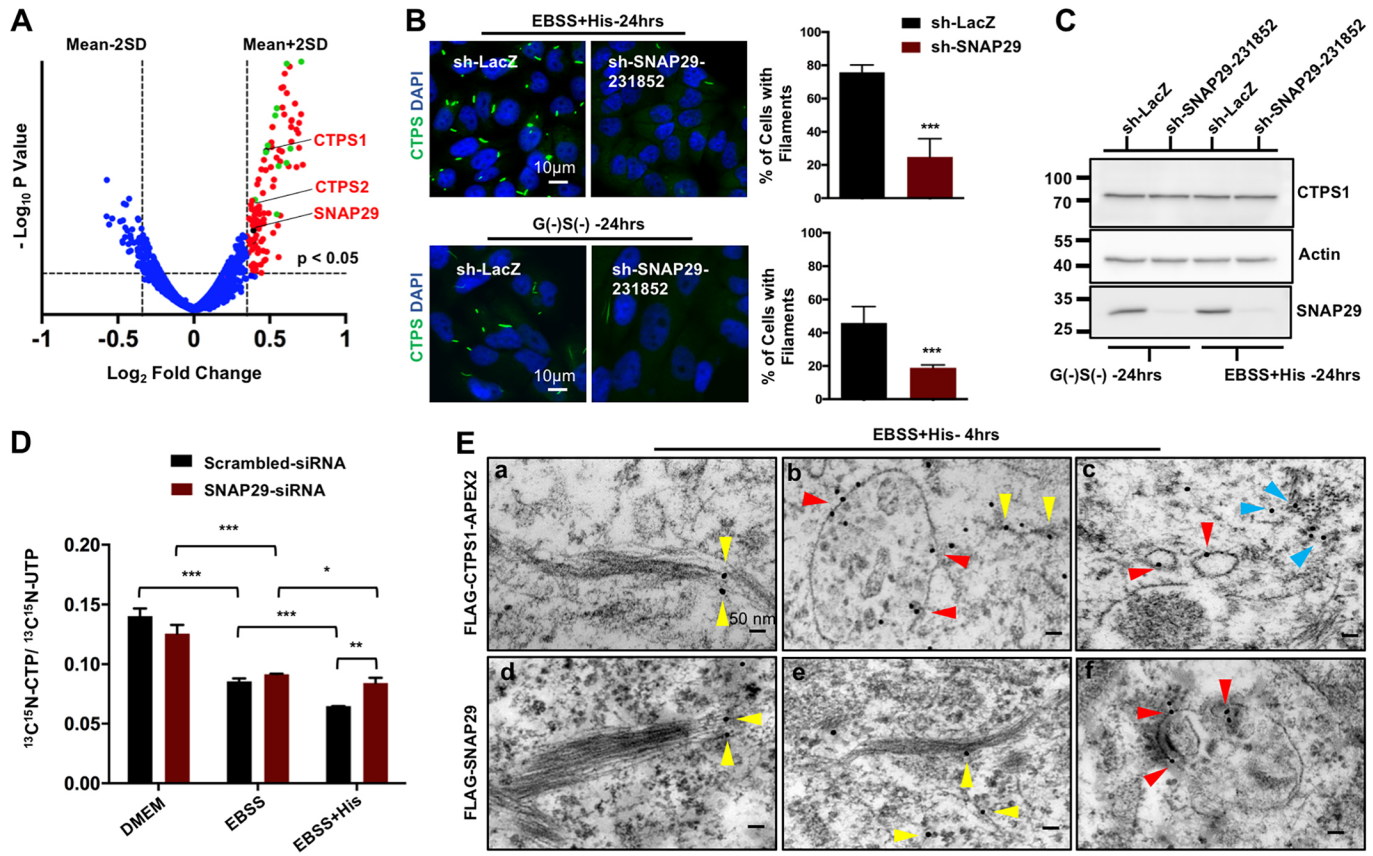

Fig. 2. SNAP29 is involved in CTPS filament formation. (A) A volcano plot comparing the $\log_2$ fold changes (*x*-axis) versus the $-\log_{10}$ *P* values (*y*-axis) for each protein identified in the 6-plex TMT-labeled proteomic profiling of HEp-2 cells expressing FLAG–CTPS1–APEX2 cultured in EBSS and EBSS+His at 6 h. Proteins marked in black (CTPS1, CTPS2 and SNAP29), green (KRT proteins: 9, 6A, 6B, 16, 5, 14, 1b, 1, 3, Hb4, 23, 78, 10, 2 and Ha6) and red are significantly enriched during CTPS filament formation. (B) shRNA-mediated SNAP29 knockdown in HEp-2 cells led to reduced CTPS filament formation in EBSS+His (50 µM) and G(−)S(−) conditions. The percentage of cells bearing CTPS filaments was calculated for three independent experiments. shRNA against LacZ (sh-LacZ) was used as a control. Results are mean±s.d. ***P<0.001 (Student's *t*-test). (C) Western blotting analysis of CTPS and SNAP29 protein levels in sh-LacZ and sh-SNAP29 knockdown HEp-2 cells for G(−)S(−) and EBSS+His 50 µM conditions at 24 h. (D) SNAP29 knockdown HEp-2 cells were cultured in DMEM, EBSS or EBSS+His for 6 h followed by treatment with $^{13}C^{15}N$-uridine (100 µM) for 1 h. The ratio of labeled CTP to labeled UTP is shown. Results are mean±s.d. *P<0.05, **P<0.01, ***P<0.001 (Student's *t*-test). (E) (a–c) Electron micrograph of FLAG gold labeling in HEp-2 cells transfected with FLAG–CTPS1–APEX2. CTPS filaments were induced through culture in EBSS+His medium for 4 h. Arrowheads point to the 18-nm Gold FLAG. ImmunoEM revealed FLAG labeling on filament-like structures (yellow arrowheads), cross-sections of the filament (blue arrowheads) and on the membrane structure (red arrowheads). (d–f) Electron micrograph of FLAG gold labeling in HEp-2 cells transfected with FLAG–SNAP29. CTPS filaments were induced through culture in EBSS+His medium for 4 h. Arrowheads point to the 18-nm gold FLAG. ImmunoEM revealed FLAG labeling on filament-like structures (yellow arrow) and membrane structures (red arrowheads) as a positive control.

K71–K80, K81–K86) intermediate filaments, and they form obligate heterodimers (Loschke et al., 2015). Keratins have been shown to be involved in the stress response, such as the role of keratin 8 (KRT8) in autophagy under oxidative stress (Baek et al., 2017). We decided to knockdown a few of the epithelial keratins identified in our proteomic analysis and found that shRNA-mediated knockdown of KRT8 significantly reduced the formation of CTPS filaments (Fig. 3C,D; Fig. S5A,C). K8 and K18 are most common in simple epithelia; they form a network via the assembly of heterodimers into non-polar unit-length filaments (ULF) and into intermediate filaments (Snider and Omary, 2014; Windoffer et al., 2011). However, knockdown of KRT18 in HEp-2 cells did not affect CTPS filament formation (Fig. 3C,D; Fig. S5B,C). Partial knockdown of KRT8 significantly reduced the cytokeratin network in HEp-2 cells when immunostained using a pan-cytokeratin antibody (Fig. S5D). By contrast, knockdown of KRT18 did not reduce the fluorescence intensity of the cytokeratin network (Fig. S5D), suggesting that KRT18 might be redundant, as KRT8 can interact with other keratins. The fold changes for KRT8 and KRT18 in the TMT labeling assay were not significant enough for them to be identified as candidates for being His-regulated CTPS interactors, possibly due to their abundant interaction with CTPS under both EBSS and EBSS+His conditions.

To further understand the proximity of CTPS to cytokeratin, we used a PLA. We found that both the keratin isotypes KRT8 and KRT18, were close to CTPS (Fig. 3E), and SNAP29 was also close to KRT8 (Fig. 3E), suggesting a possible interaction of SNAP29 and CTPS on cytokeratin. Immunofluorescence imaging confirmed the colocalization of GFP-tagged CTPS with mCherry-tagged KRT8 and KRT18 (Fig. 3F; Fig. S5E) and also endogenous CTPS with KRT8 in HEp-2 cells (Fig. S5F). Similarly, in HEK 293T cells, FLAG–CTPS1–GFP filaments were colocalized with mCherry-tagged KRT18 under DON treatment (Fig. S5G). We used mCherry–KRT18 or mCherry–KRT8 together with FLAG–CTPS1–GFP to monitor CTPS filament assembly in live cells under EBSS+His conditions. Live imaging of these cells revealed an association between CTPS1 and the KRT8–KRT18 network

Journal of Cell Science (2020) 133, jcs240200. doi:10.1242/jcs.240200

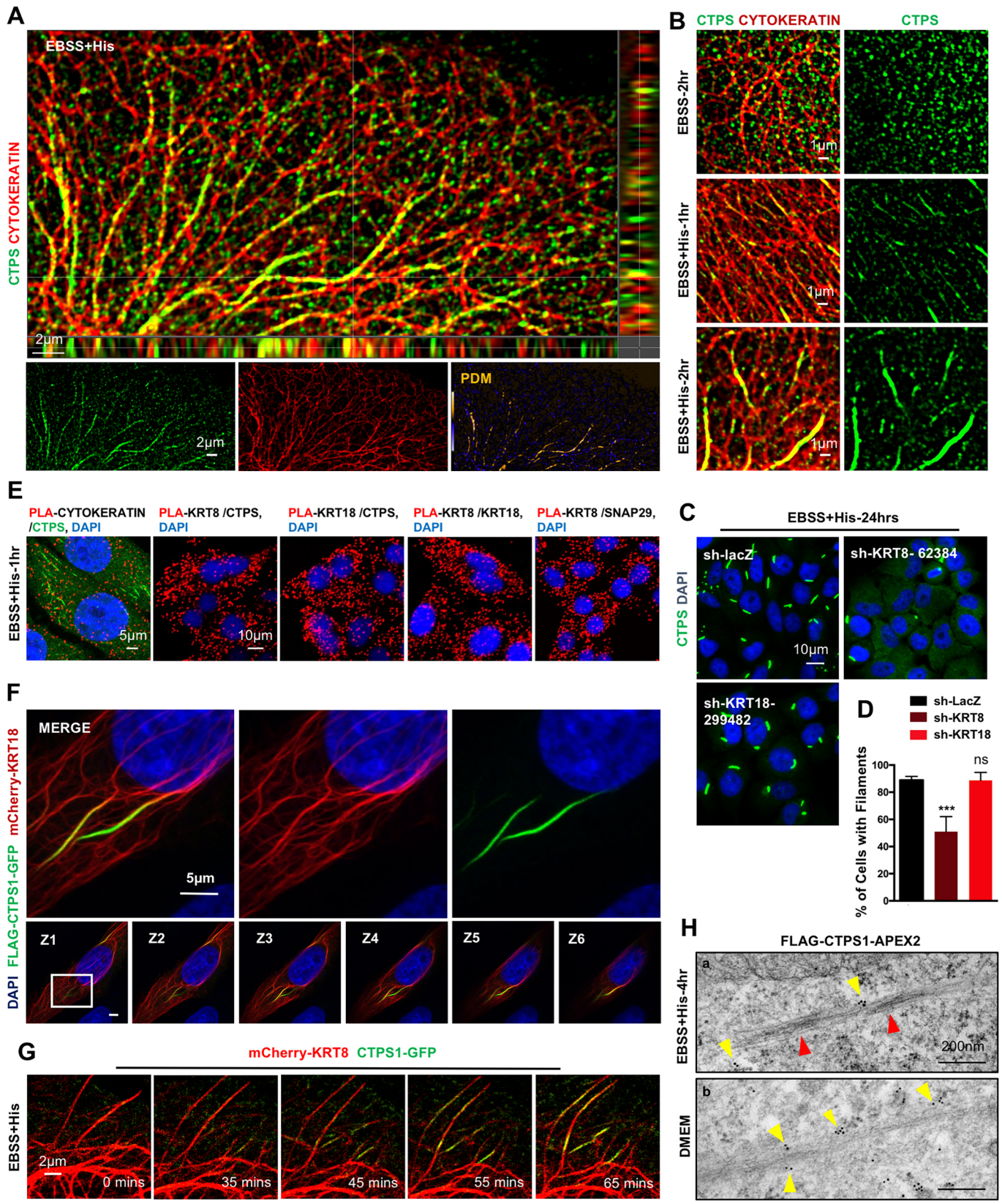

Fig. 3. See next page for legend.

(Movies 1–3). A longer imaging time showed that the CTPS signal grew along the cytokeratin to give thicker filaments (Fig. 3G; Fig. S5H, Movies 2 and 3). Furthermore, using EM, we found that gold labeling of endogenous KRT8 can be detected on DAB-stained FLAG–CTPS–APEX2 filaments in HEp-2 cells (Fig. 3H; Fig. S6A). As expected, the percentage of KRT8 immunogold on

Fig. 3. CTPS assembles along the cytokeratin network. (A) Super-resolution image of CTPS and cytokeratin in the EBSS+His condition shows their colocalization at a single *Z*-section. Cytokeratin was immunostained using anti-pan-cytokeratin (red) antibodies, and CTPS was immunostained with anti-CTPS (green) antibodies. In the product of the differences from the mean (PDM) images, each pixel represents the PDM value at a location as shown by the PDM scale bar. Yellow represents a positive PDM value, and purple represents a negative PDM value. (B) Time-dependent assembly of CTPS on cytokeratin in EBSS+His conditions. HEp-2 cells were immunostained with anti-CTPS (green) and anti-pan cytokeratin (red). (C,D) Representative images of CTPS filaments in HEp-2 cells with shRNA-mediated knockdown of KRT8 and KRT18. The percentage of cells bearing CTPS filaments was calculated for three independent experiments. Results are mean±s.d. ***P<0.001; ns, not significant (Student's *t*-test) (D). (E) PLA between CTPS and cytokeratin (pan-cytokeratin; KRT8 and KRT18), between KRT18 and KRT8, and between KRT8 and SNAP29 in EBSS+His conditions at 1 h. After PLA, HEp-2 cells were immunostained for 30 min with secondary antibody to detect CTPS (first panel) in the EBSS+His conditions. (F) FLAG–CTPS1–GFP colocalized with mCherry–KRT18 in the EBSS+His condition at 6 h. The square box represents the enlarged region; Z represents a single *Z* plane for the confocal imaging. (G) Live imaging of GFP-tagged CTPS1 filaments during the process of assembly. HEp-2 cells expressing FLAG–CTPS–GFP (green) and mCherry–KRT8 (red) were imaged with the Nikon Ti2 Dragonfly High Speed confocal platform every 5 min for 65 min (Movie 2). Prior to imaging, cells were incubated in EBSS+His conditions for 1 h. (H) Electron micrograph of KRT8 gold labeling in HEp-2 cells transfected with FLAG–CTPS–APEX2 in (a) EBSS+His and (b) DMEM. ImmunoEM revealed KRT8 labeling (yellow arrowheads) along DAB-stained FLAG-CTPS-APEX2 filaments (red arrowheads). DAB staining in DMEM did not show any positive signal for CTPS filaments.

filament-like structures did not change between DMEM and EBSS+His conditions (Fig. S6B).

Moreover, we found that disrupting the cytokeratin network with 8% 1,6-hexanediol (1,6-HD) dissembled the CTPS filaments completely within a few minutes (Fig. 4A–C) (Lin et al., 2016). However, the possibility that 1,6-HD dissembles CTPS filaments directly was not excluded based on our results. It was interesting that when cells recovered for an hour in EBSS+His medium after 10 min of treatment with 1,6-HD, CTPS filaments were observed adjacent to the reformed keratin filaments (Fig. 4C). Other cytoskeletal proteins, such as actin and tubulin, showed no colocalization with CTPS filaments, and their disruption had no effect on CTPS filament formation (Fig. 4D–F), which is consistent with results from a previous study (Carcamo et al., 2011).

Stress induces a spatiotemporal interaction between SNAP29 and the cytokeratin network

Since PLA signals were detected for both CTPS and SNAP29 with cytokeratin (Fig. 3E), we tested whether SNAP29 affects the assembly of CTPS on cytokeratin. In SNAP29-knockdown cells, dotted CTPS signals were detected after 1 h of His induction, whereas in control cells, numerous CTPS filaments were already assembled along the cytokeratin network (Fig. 5A). Furthermore, single *Z*-section imaging showed that the PLA signal of CTPS and Flag–SNAP29 was located proximal to the cytokeratin network (Fig. 5B). To understand this association, we C-terminally tagged KRT18 with APEX2 to biotinylate the cytokeratin network, which is assumed to be the platform where CTPS filament assembly-related events occur (Fig. S6C). ImmunoEM anti-Flag gold labeling detected FLAG–CTPS–GFP along DAB-stained KRT18–APEX2 filaments in HEp-2 cells during the CTPS filament formation process (Fig. 5C; Fig. S6D). The percentage of Flag immunogold labeling on KRT18 DAB-stained filaments was significantly increased in EBSS+His condition when compared to the DMEM condition (Fig. S6E). Furthermore, KRT18–APEX2 revealed that the proximity of SNAP29 to the cytokeratin network increased spatiotemporally in response to stress (Fig. 5D; Fig. S6F). To confirm that SNAP29 availability can affect the process of CTPS filament assembly, we used N-ethylmaleimide (NEM), a non-selective thiol alkylator that has been reported to inhibit SNARE recycling and trap SNAP29 in the SNARE complex (Abada et al., 2017; Glick and Rothman, 1987). Indeed, we found that NEM treatment in HEp-2 cells led to the rapid fragmentation of CTPS filaments within 5 min without disrupting the cytokeratin network (Fig. 5E; Fig. S6G), suggesting that SNAP29 availability might be important for CTPS filament formation and maintenance. KRT18–APEX2-mediated proximity labeling showed that SNAP29 proximity to the cytokeratin network increased with NEM treatment, which was added during the last 10 min of biotin labeling (Fig. 5F). Using super-resolution imaging, we found a considerable amount of SNAP29 signal associated with the cytokeratin network, which increased with NEM treatment (Fig. 5G,H). Consistent with this, more SNAP29 was co-immunoprecipitated with KRT8 upon NEM treatment (Fig. 5I). Super-resolution imaging suggests that during CTPS filament formation, SNAP29 interacts with CTPS along cytokeratin network (Fig. 5Ja–e). It is plausible that with NEM treatment, SNAP29 recycling along the cytokeratin network is impaired, leading to its reduced availability for CTPS filament assembly and maintenance (Fig. 5Jf–j). Taken together, our data suggest that CTPS filament formation is dynamic and might be regulated by a balance of assembly and disassembly, in which NEM could intervene. Moreover, this assembly along cytokeratin might require proper conformation of the CTPS protein, because the G148A CTPS mutant, which cannot form tetramers could not assemble on the cytokeratin network (Fig. S6H), which is consistent with results from previous studies (Barry et al., 2014; Huang et al., 2017; Lin et al., 2018; Noree et al., 2014).

DISCUSSION

Here, we report that human CTPS filaments are compartmentalized along the cytokeratin network during nutrient starvation stress. We found that in response to stress, SNAP29 interacts spatiotemporally with the cytokeratin network. This availability of SNAP29 near the cytokeratin network might play a key role in CTPS filament formation and/or maintenance. In addition, SNAP29 is required for the regulation of CTPS enzymatic activity through protein assembly. We also found that IMPDH2 compartmentalizes along the cytokeratin network under glutamine and serum starvation, suggesting that during stress, cytokeratin might serve as a site for the compartmentalization of important metabolic enzymes, modulating their activity by polymerization (Lin et al., 2018).

In *Caulobacter crescentus*, CtpS has been reported to serve as a cytoskeletal filament to regulate cell curvature through interacting with a cell-shape regulator protein, crescentin, which has intermediate filament-like properties (Ingerson-Mahar et al., 2010). In humans, there are six types of intermediate filament that are widely categorized on the basis of sequence identity (Snider and Omary, 2014). Cytokeratins, which represent the largest family among all types of intermediate filaments, are the most diversified intermediate filament members. They have been reported to be involved in stress responses (Baek et al., 2017; Maruthappu et al., 2017; Snider and Omary, 2014), and now we have shown that knockdown of KRT8 interferes with the assembly of CTPS filaments under Gln deprivation stress. Immunofluorescence imaging and inhibitor treatment indicated that actin and microtubules do not associate with CTPS filaments (Fig. 4D–F).

Journal of Cell Science (2020) 133, jcs240200. doi:10.1242/jcs.240200

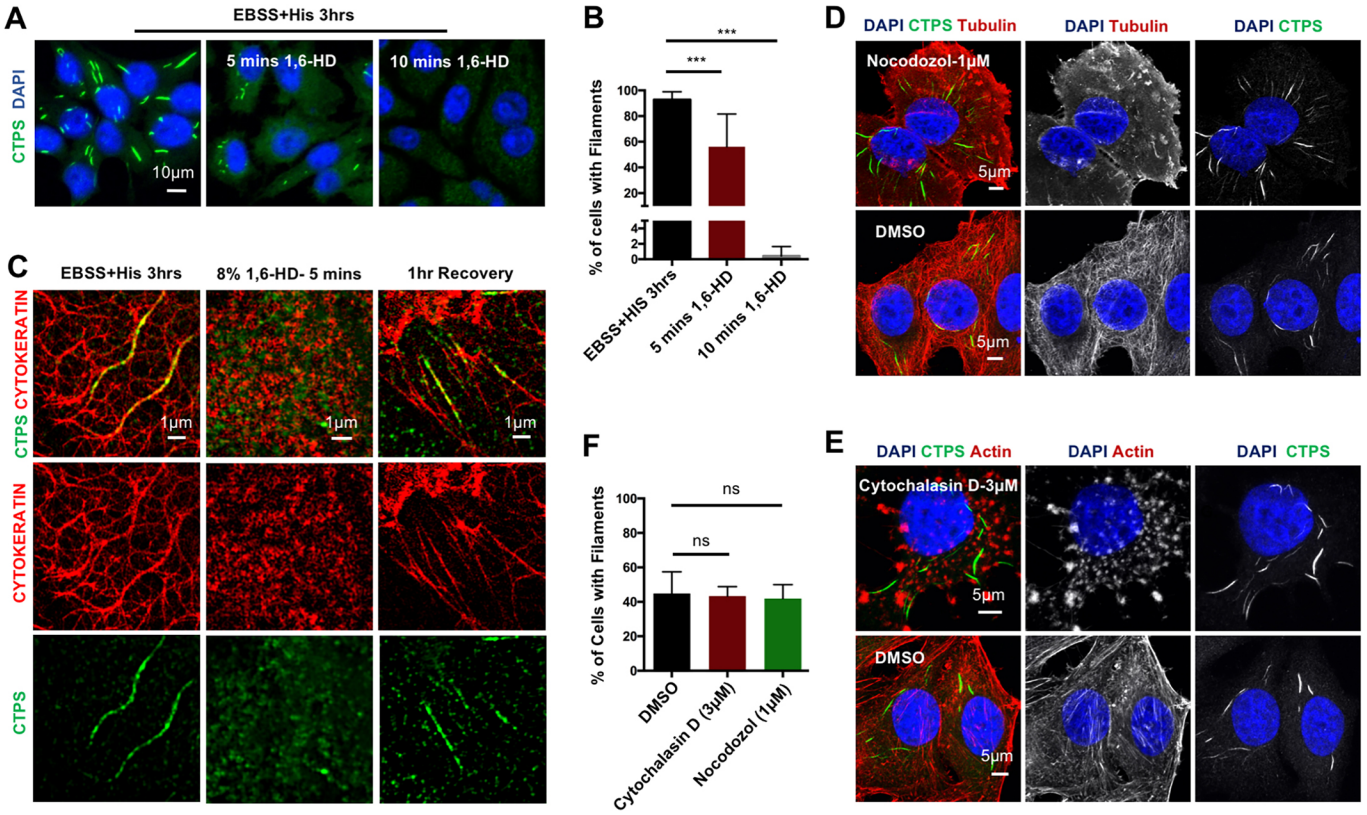

Fig. 4. CTPS filament formation is affected by cytokeratin disassembly. (A,B) HEp-2 cells were incubated with EBSS+His conditional medium for 3 h to induce CTPS filaments prior to 8% 1,6-hexanediol treatment for 5 min and 10 min. The percentage of cells bearing CTPS filaments was calculated for three independent experiments. Results are mean±s.d. ***P<0.001 (Student's t-test). (C) Treatment with 8% 1,6-HD for 5 min dissembled the cytokeratin network and also reduced the CTPS filaments. After complete disassembly of CTPS filaments (i.e. after 10 min of 8% 1,6-HD treatment), HEp-2 cells were allowed to recover in EBSS+His conditional medium for 1 h. The cytokeratin network was not completely recovered, although thin CTPS filaments were formed, which were still assembled along the cytokeratin network. (D–F) HEp-2 cells were pre-incubated with nocodazole (1 μM)/cytochalasin D (3 μM)/DMSO in EBSS medium for 1 h before stimulation with His for another 1 h in the same medium. The percentage of cells bearing CTPS filaments was calculated for three independent experiments. Results are mean±s.d. ns, not significant (Student's t-test).

Moreover, simultaneous assembly and disassembly of the cytokeratin network and CTPS filaments were observed with the addition and removal of 1,6-HD, respectively (Fig. 4C) (Lin et al., 2016). These results suggested a possibility that CTPS filament formation is related to the cytokeratin network.

The combination of the APEX approach and His induction system allowed us to identify proteins that are not only adjacent to the CTPS filaments but also interact dynamically with CTPS, and hence could be involved in the process of filament formation. However, the enrichment of these two types of proteins depends on the dynamic nature of filament formation, given that CTPS filament formation is not synchronized in every cell. SNAP29, one of three candidates identified to regulate CTPS filament formation from our initial screen (Fig. 1E–G; Fig. S2F), was also verified in the repeat TMT analysis (Fig. 2A) and was found to co-immunoprecipitate with KRT8 (Fig. 5I). According to the results of KRT18–APEX2-based proximity analysis, immunofluorescence imaging of the SNAP29–CTPS filament–cytokeratin network, and the effects of NEM treatment, we proposed a model in which stress-dependent availability of SNAP29 on the cytokeratin network facilitates the assembly of CTPS into filamentous structures along these networks (Fig. 6). Indeed, several roles of intermediate filament proteins have recently emerged in the regulation of vesicle trafficking (Margiotta and Bucci, 2016). The contribution of histidine to the methionine cycle, and that methylation is required for filament formation, were demonstrated in our previous study (Lin et al., 2018). We think that SNAP29 function in CTPS filament formation requires histidine-mediated effects, which could be post-translational modifications of the CTPS protein or other filament-related proteins. It is well known that post-translational modification is critical for functions of the cytokeratin network (Snider and Omary, 2014). Interestingly, according to the KRT18–APEX2 results, the proximity between keratin 18 and CTPS was not significantly altered by stress during filament formation, suggesting that SNAP29 does not directly affect the relative location of CTPS in the cytokeratin network. The detailed molecular mechanism of CTPS filament assembly needs further investigation. Our present study might also further shed light on the CEDNIK condition, given that loss of SNAP29 function leads to defective skin development (Mastrodonato et al., 2018).

MATERIALS AND METHODS

Mammalian cell culture

Human HEp-2, HeLa and HEK 293 cells were cultured in in Dulbecco's modified Eagle's Medium (DMEM) (GIBCO) supplemented with 10% fetal bovine serum (FBS) and 1× antibiotic-antimycotic (GIBCO) at 37°C under 5% CO_2.

Antibodies and reagents

The antibodies were anti-pan-cytokeratin (Abcam, cat. no. ab86734), anti-tubulin antibody (Abcam, cat. no. ab6160), SNAP29 antibody (GeneTex, cat. no. GTX131028), anti-SNAP29 antibody (Abcam, cat. no. ab181151),

Journal of Cell Science (2020) 133, jcs240200. doi:10.1242/jcs.240200

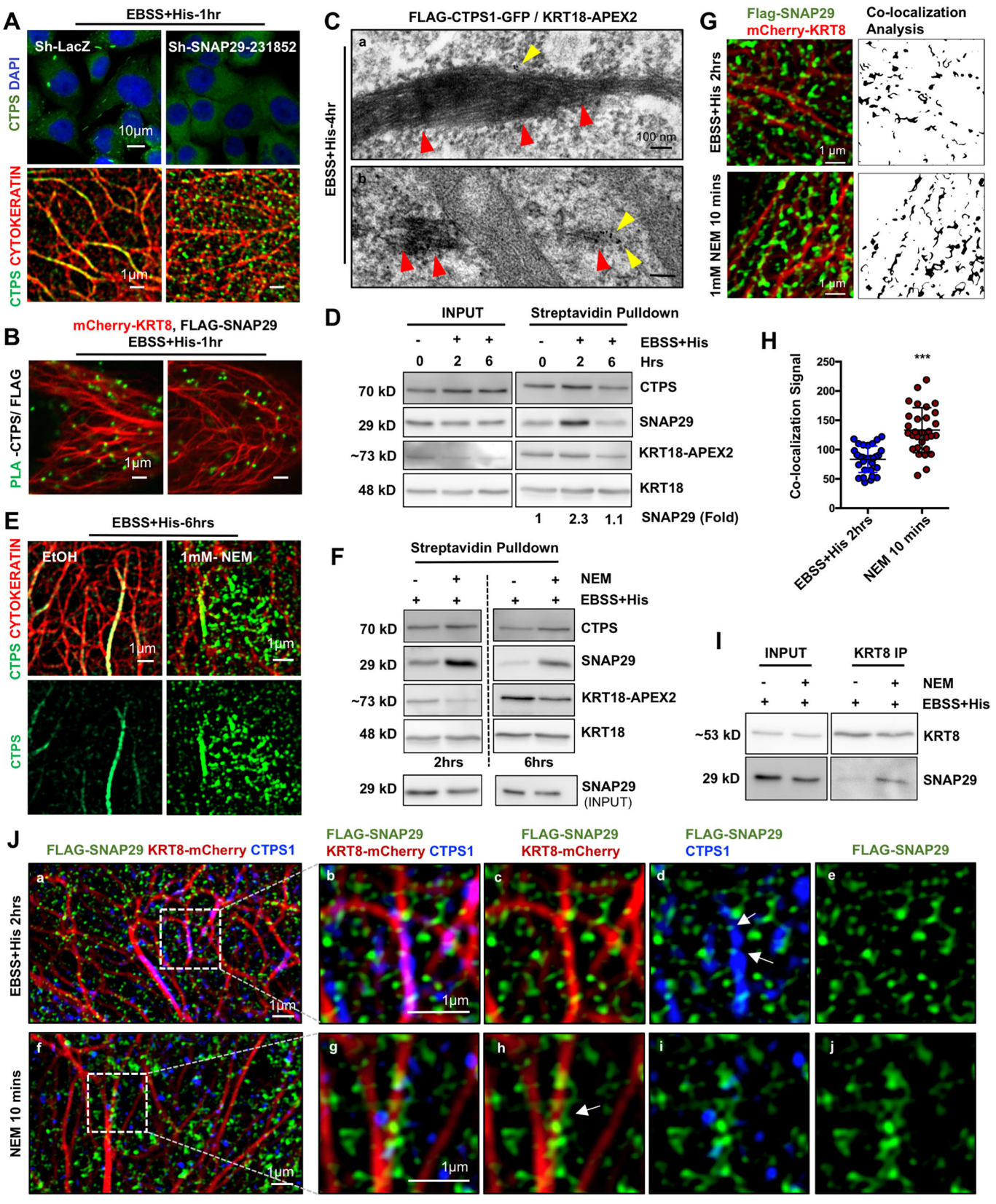

Fig. 5. See next page for legend.

anti-IMPDH2 (Proteintech, cat. no: 12948-1-AP), anti-CTP synthase (Santa Cruz Biotechnology, cat. no. sc-134457), anti-CTPS antibody (GeneTex, cat. no. GTX105265), anti-KRT18 antibody (Santa Cruz Biotechnology, cat. no. sc-6259), anti-KRT8 antibody (Santa Cruz Biotechnology, cat.no. sc-8020), anti-KRT8 antibody (Proteintech, cat.no. 10384-1-AP), donkey polyclonal secondary antibody to mouse IgG - H&L (Abcam, cat. no.

Fig. 5. SNAP29 interacts with cytokeratin and is required for CTPS filament assembly along cytokeratin. (A) sh-SNAP29 and sh-LacZ stable knockdown HEp-2 cells were incubated for 1 h in EBSS+His conditions followed by immunostaining with anti-pan-cytokeratin (red) and anti-CTPS (green) antibodies. Super-resolution images are from the respective conditions. (B) PLA between CTPS and FLAG in EBSS+His conditions at 1 h. HEp-2 cells were transfected with FLAG–SNAP29 and mCherry–KRT8 before the medium was replaced with EBSS+His for 1 h. Images are single *z* sections showing PLA signals adjacent to the cytokeratin track. Two examples are shown. (C) Two electron micrographs of FLAG gold labeling in HEp-2 cells transfected with FLAG–CTPS–GFP and KRT18–APEX2 in EBSS+His. ImmunoEM revealed FLAG labeling (yellow arrowheads) along DAB-stained KRT18–APEX2 filaments (red arrowheads). (D) Time-dependent enrichment of SNAP29 in the EBSS+His group. HEp-2 cells were transfected with KRT18–APEX2, and biotinylated proteins at 0 h, 2 h and 6 h after CTPS filament induction were immunoprecipitated (IP) using streptavidin-conjugated magnetic beads. Band intensity of streptavidin pulldown of SNAP29 was normalized against that of streptavidin pulldown of KRT18–APEX2, and the fold change for SNAP29 was measured by normalizing all groups (0 h, 2 h and 6 h) against 0 h. 3.4% of the total sample was used as loading control. (E) Super-resolution image of a CTPS filament in the process of disassembly when treated with 1 mM NEM. CTPS filaments were induced in EBSS+His for 6 h before dissembling with 1 mM NEM for 5 min. (F) SNAP29 enrichment increased with NEM treatment. HEp-2 cells were transfected with KRT18–APEX2, and biotinylated proteins at 2 h and 6 h after CTPS filament induction were immunoprecipitated using streptavidin-conjugated magnetic beads. Cells were treated with 1 mM NEM for 10 min before initiating APEX2-mediated biotin labeling by treatment with H_2O_2 for 1 min. (G,H) Super-resolution images (G) of FLAG–SNAP29 (green) and mCherry–KRT8 (red) in EBSS+His conditions at 2 h. NEM at 1 mM applied during the last 10 min of the 2-h incubation increased the SNAP29 signal along the cytokeratin network. Pseudo-colored images represent colocalization signal determined using ImageJ software. To quantify the colocalization signal (H), random images (n=30) of 10 cells from each group were acquired using ELYRA PS.1 super-resolution microscopy and were further subjected to colocalization analysis using ImageJ software. The mean±s.d. is indicated. ***P<0.001 (Student's *t*-test). (I) Endogenous SNAP29 can be co-immunoprecipitated (IP) with endogenous KRT8 using anti-KRT8 antibody. NEM treatment increased the amount of SNAP29 co-immunoprecipitated with KRT8. HEp-2 cells were treated with 1mM NEM for 10 min after 2 h of filament induction in the EBSS+His condition. 1.5% of the total sample was used as loading control. (J) (a–e) Super-resolution image of CTPS (blue), FLAG–SNAP29 (green) and mCherry–KRT8 (red) in EBSS+His conditions at 2 h. Magnified images (b–e) show SNAP29 interacts with CTPS filaments along the cytokeratin network at intervals. (f–j) NEM treatment aggregated SNAP29 along the cytokeratin network. HEp-2 cells were treated with 1 mM NEM for 10 min after 2 h of filament induction. White arrowheads showing SNAP29 aggregation along cytokeratin. Magnified images (g–j) show clustered SNAP29 along the cytokeratin network.

ab105278), monoclonal ANTI-FLAG® M2 antibody (Sigma-Aldrich, cat. nos F3165 and F1804), streptavidin–Alexa Fluor 488 conjugate (Thermo Fisher Scientific, cat.no. S11223), Alexa Fluor 488–Phalloidin (Thermo Fisher Scientific, cat. no. A12379) and EasyBlot anti rabbit IgG conjugated to HRP (GeneTex, cat. no. GTX221666-01). Dilutions used are provided in Table S4. The pharmacological inhibitors used were nocodazole (Sigma-Aldrich, cat.no. M1404), cytochalasin D (Thermo Fisher Scientific, cat.no. PHZ1063), 1,6-hexanediol (Sigma-Aldrich, cat.no. 240117), 6-diazo-5-oxo-L-norleucine (DON) (Sigma-Aldrich, cat.no. D2141) and N-ethylmaleimide (NEM) (Sigma-Aldrich, cat.no. E3876) at concentration and duration as indicated in figure legends.

Plasmids and cloning

As mentioned in Lin et al. (2018), APEX2 was cloned from 'APEX2-Actin in pEGFP' (Addgene plasmid # 66172, deposited by Alice Ting) and inserted into the BamHI site of the p3xFlag-CTPS1-CMV26 vector to generate the p3xFlag-CTPS1-APEX2-CMV26 vector. For the p3xFlag-APEX2-CMV26 vector, APEX2 was cloned from p3xFlag-CTPS1-APEX2-CMV26 and inserted into an empty p3xFlag-Myc-CMV26 with NotI and BamHI to generate the p3xFlag-APEX2-CMV26 vector. For the generation of the p3xFlag-CTPS1-GFP-CMV26 vector, GFP was cloned from the pLVX-EF1alpha-CTPS-AcGFP-N1 vector [A206K was mutated in AcGFP to prevent dimer formation (Chang et al., 2018; Zacharias et al., 2002)] and inserted into p3xFlag-CTPS1-APEX2-CMV26 with BamHI sites to replace APEX2 with GFP. Human SNAP29, KRT18 and KRT8 were amplified from RNA extracted from HEp-2 cells. SNAP29 was inserted into p3xFlag-Myc-CMV26 with NotI and XbaI sites to generate the p3xFlag-SNAP29-CMV26 vector. For the generation of the siRNA-resistant SNAP29 construct, three nucleotides were point mutated (A678G, T681C and G684A) on the siRNA recognition site. Primers for site-directed mutagenesis were designed using QuikChange primer design tool (Agilent). KRT18 and KRT8 were inserted into pmCherry-N1 (Addgene #54517) with NheI and HindIII sites to generate pmCherry-KRT18 and pmCherry-KRT8. CTPS2 was cloned from HEp-2 cell RNA extract and inserted into empty p3xFlag-Myc-CMV26 vector with XbaI and BamHI to generate p3xFlag-CTPS2-CMV26. For the generation of the CTPS1-APEX2-MIGR1 vector, CTPS-APEX2 was cloned from the p3xFlag-CTPS1-APEX2-CMV26 vector using the XhoI site and inserted into the empty MIGRI vector (a gift from Chien-Kuo Lee, Graduate Institute of Immunology, National Taiwan University, Taiwan). For the generation of the KRT18-APEX2 vector, APEX2, including the stop codon, was cloned from the p3xFlag-CTPS1-APEX2-CMV26 vector using the HindIII site and inserted into the pmCherry-KRT18 vector. For exogenous expression, 5×10^5 cells were transfected at 60–70% confluence using Lipofectamine 2000 (Invitrogen) following the manufacturer's instructions.

Lentivirus infection for stable gene knockdown

Lentiviral shRNAs targeting LacZ (TRCN0000072224), SNAP29 (TRCN0000231852, TRCN0000381551), CAPG (TRCN0000029463), UBL5 (TRCN0000011115), KRT8-(TRCN0000062384), KRT18 (TRCN0000299482) and other candidate genes were purchased from RNAi core (NCR), Academia Sinica, Taiwan. A total of 6×10^5 cells were infected with 3.6×10^6 colony forming units (CFU)/ml recombinant viral fluid together with 8 µg/ml of polybrene. At 24 h post infection, cells were replaced with fresh medium containing 2 µg/ml puromycin. The selection process was repeated one more time before establishing the stable gene knockdown cell line. RT-qPCR primers were as follows: SNAP29 (FW, 5′-CCTGAACAG-AATGGCACCCT-3′; REV, 5′-TGGGGACAGGGTCTGTATCA-3′); UBL5 (FW, 5′-AGCTGATTGCAGCCCAAACT-3′; REV, 5′-TCGTGTACCACT-TCTTCAGGACAA-3′), and CAPG (FW, 5′-CCTGAACAGAATGGCAC-CCT-3′; REV, 5′-TGGGGACAGGGTCTGTATCA-3′).

Immunostaining for mammalian cells

For immunostaining, 6×10^4 HEp-2 cells were seeded in 100-mm non-treated glass cover slips in 24-well plates for 24 h. To induce CTPS filaments, the cell culture medium was replaced with conditional medium [EBSS, EBSS+His (200 µM concentration of His, unless otherwise mentioned); denoted G(−)S(−)]. Cells were washed twice with 1× PBS and fixed with fixation buffer (4% formaldehyde and 4% sucrose diluted in 1× PBS) for 10 min. The fixed cells were then washed twice with 1× PBS and permeabilized with 100% ice cold (−20°C) methanol or acetone at room temperature for 2 min. Subsequently, the cells were again washed twice with 1× PBS and blocked in blocking buffer (3% BSA and 0.2% Triton X-100 in 1× PBS) at room temperature for 20 min before incubating with primary antibody diluted in blocking buffer (without 0.2% Triton X-100) overnight at 4°C. The cells were washed three times for 5 min each with 'Wash buffer' (1× PBS containing 0.2% Tween-20) and incubated with secondary antibody for 1 h at room temperature. Subsequently, the cells were washed three times with wash buffer for 5 min each, and then the cells were mounted on glass plates with multi medium containing DAPI.

Quantitative proteomic analysis using iTRAQ

Biotin phenol labeling in live cells

Cells transfected with FLAG–CTPS1–APEX2 or FLAG–APEX2 were incubated in EBSS or EBSS+His (200 µM) for 6 h at 36 h post transfection. For the EBSS+His+Gln group, cells were initially incubated under

Journal of Cell Science (2020) 133, jcs240200. doi:10.1242/jcs.240200

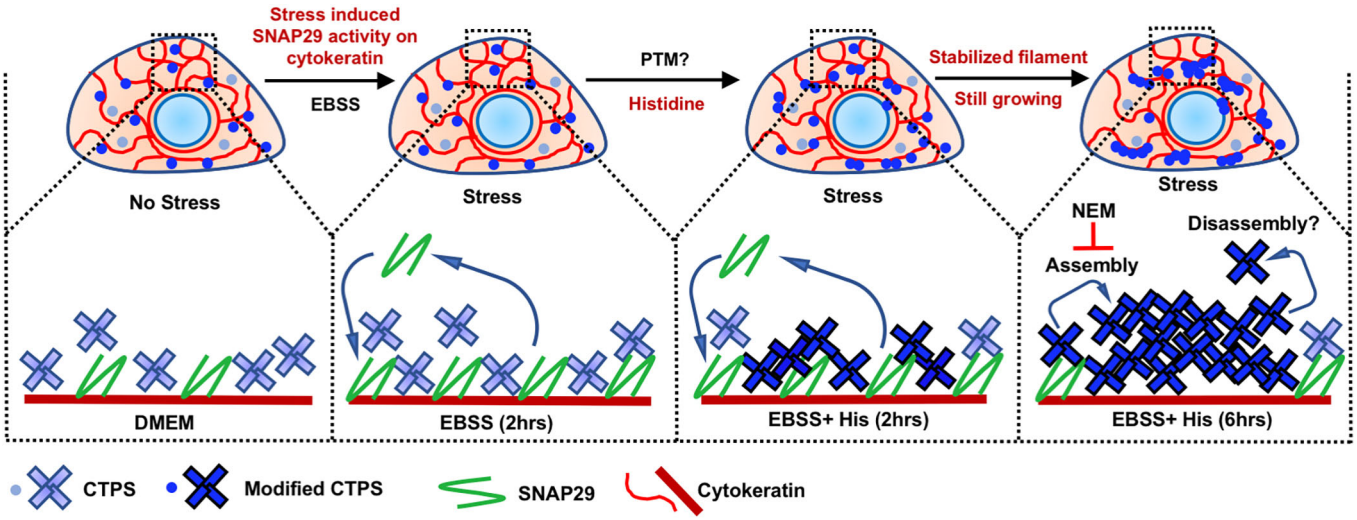

Fig. 6. Model for CTPS filament assembly. In DMEM conditions, CTPS and SNAP29 are in proximity to the cytokeratin network. During early stages of EBSS or EBSS+His stress (~ 2 h), SNAP29 interaction with cytokeratin increases. However, as in EBSS+His conditions, CTPS might be post-translationally modified (Lin et al., 2018) or have a conformation change (tetramer mutant), leading to its SNAP29-mediated assembly along the cytokeratin network. The presence of a larger pool of SNAP29 along the cytokeratin might facilitate CTPS assembly into filaments. However, at later time points (~ 6 h), this enrichment of SNAP29 gradually drops, while the assembly and disassembly of CTPS filaments is in balance.

EBSS+His conditions, and during the last 15 min of the 6-h incubation, 4 mM Gln was added dropwise to the medium. After 6 h of incubation, each group was replaced with their corresponding conditional medium containing 500 µM biotin phenol (Iris Biotech, LS3500). Cells were further incubated at 37°C under 5% CO_2 for 30 min and then treated with H_2O_2 (at a final concentration of 1 mM) for 1 min. The reaction was quenched using a quencher solution containing 10 mM sodium ascorbate (A7631, Sigma-Aldrich), 10 mM sodium azide (S2002, Sigma-Aldrich) and 5 mM Trolox (238813, Sigma-Aldrich). Cells were subsequently processed for immunostaining or immunoprecipitation.

Immunoprecipitation of biotinylated proteins

After biotin labeling, cells were scraped using denaturing lysis buffer (1% SDS, 50 mM Tris-HCl pH 7.4 and 5 mM EDTA) containing 1× protease inhibitor cocktail (Complete Mini, Roche) at room temperature to completely denature the proteins. Afterwards, non-denaturing buffer (1% Triton X-100, 50 mM Tris-HCl pH 7.4, 300 mM NaCl and 5 mM EDTA) was added to the lysed samples to dilute the SDS concentration to 0.1%. Subsequently, experimental groups were sonicated, and protein concentrations were measured using the Bradford method (Protein Assay, Bio-Rad). Biotinylated proteins were then pulled down using streptavidin-coated magnetic beads (Pierce, cat. no. 88816). To detect biotinylated proteins by western blot analysis, the blot was blocked with 5% BSA in Tris-buffered saline containing 0.1% Tween 20 overnight at 4°C and later incubated with streptavidin–HRP (Thermo Scientific, cat. no. 21126) for 1 h at room temperature. The blot was further washed in blocking buffer five times for 5 min each before developing with Western Lightning ECL Pro (PerkinElmer).

Trypsin digestion for iTRAQ labeling

Immunoprecipitated biotinylated proteins were eluted from the streptavidin-coated magnetic beads using 0.1% trifluoroacetic acid (TFA)/50% acetonitrile (ACN) and dried in a Speed-Vac followed by in-solution digestion. Samples were dissolved in 250 mM triethylammonium bicarbonate (TEABC) and then reduced with 5 mM tris(2-carboxyethyl)-phosphine (TCEP) at 60°C for 1 h. Further samples were alkylated with 10 mM methyl methanethiosulfonate (MMTS) for 30 min at room temperature and subsequently digested with sequencing grade modified porcine trypsin (20 µg/ml) (Promega) overnight at 37°C. Tryptic digested peptides were dried by Speed-Vac for further iTRAQ labeling. Tryptic digested peptides were dissolved in 50 mM TEABC and then labeled with iTRAQ reagent (Applied Biosystems) for 1 h at room temperature. Labeled peptides were mixed at a 1:1:1 ratio and further desalted for 2D LC-MS/MS analysis.

2D LC-MS/MS analysis and database search for the iTRAQ experiment

In Lin et al. (2018), we previously described the method for LC-MS/MS analysis and database searching. The peptide mixture for iTRAQ was separated and analyzed by 2D LC-MS/MS using a strong cation exchange (SCX) and reverse-phase C18 (RP18) liquid chromatography system on a Dionex UltiMate 3000 nano LC system coupled to a LTQ-Orbitrap Elite mass spectrometer (Thermo Fisher Scientific). The peptide mixture was reconstituted in HPLC buffer A [30% ACN and 0.1% formic acid (FA)] and loaded onto a homemade column (Luna SCX, bead size, 5 µm; column dimensions, 180×0.5 mm for iTRAQ experiment; 130×0.5 mm for label-free experiment) (Phenomenex Inc., Torrance, CA) at a flow rate of 5 µl/min for 30 min. The peptides were then fractionated into 44 fractions for iTRAQ, using a continuous HPLC buffer B gradient (0–100% of 0.5 M ammonium chloride in the presence of 30% CAN and 0.1% FA). Each fraction was then mixed with a stream of 0.1% FA in H_2O, and the peptides were trapped on a Zorbax C18 column (bead size, 5 µm; pore size, 30 nm; column dimensions, 5×0.3 mm) (Agilent Technologies Inc., Santa Clara, CA) and separated on a 60-min (for iTRAQ) linear gradient of 99.9% CAN and 0.1% FA on a Hydro RP chromatography column (bead size, 2.5 µm; pore size, 10 nm; column dimensions, 200×0.075 mm) (Phenomenex Inc.). MS/MS analysis was performed on an LTQ-Orbitrap Elite mass spectrometer. Full-scan MS spectra (m/z 400 to m/z 2000) were acquired on the mass analyzer at a resolution of 60,000 at m/z 400, followed by MS/MS of the six most intense precursor ions, above a threshold of 5000, selected for fragmentation by collision induced dissociation (CID), in addition to high-energy collision dissociation (HCD) for the iTRAQ experiment in parallel acquisition mode with a normalized collision energy setting of 35% and an activation time of 10 ms for CID and 0.1 ms for HCD. The dynamic exclusion function was set as: repeat count, 1; repeat duration, 30 s; and exclusion duration, 40 s. Proteome Discover (version1.4) (Thermo Fisher Scientific) was used to analyze and quantify MS and MS/MS data. Swiss-Prot database containing 20,205 entries for *Homo sapiens* (download in September 2015) was used for identifying the proteins. Parent and fragment ion mass tolerance for CID were set to 10 ppm and 0.5 Da and for HCD to 10 ppm and 0.05 Da, respectively. Two missed cleavages were allowed for tryptic digestion. For protein identification, oxidation of methionine, protein N-terminal acetylation and pyro-glutamination for N-terminal glutamine were set as variable modifications, whereas methylthio modification of cysteine was set as a fixed modification. Additionally, iTRAQ labeling of lysine and the

N-termini of peptides were also added. Peptide identification criteria were set as: peptide confidence, high; peptide length, 7–100; peptide maximum rank, 1; search engine rank, 1; minimal number of peptides, 2 for proteins; count only rank 1 peptide; count peptides only in top-scoring proteins; and false discovery rate (FDR) <0.01. In total, 3417 proteins were quantified. To correctly identify CTPS filament-interacting proteins, iTRAQ ratios between the experimental groups and control groups were calculated for each protein to generate three different datasets of iTRAQ ratios (i.e. 115/117, 115/114 and 115/116). We set the cutoff at the mean+1.8 s.d. to minimize the false positives (Table S1).

Quantitative proteomic analysis using TMT

Biotin-phenol labeling in live cells

Cells transfected with FLAG–CTPS1–APEX2 were incubated in EBSS or EBSS+His (200 µM) for 6 h, after 24 h of transfection in triplicate. During the last 30 min of the 6-h incubation, biotin phenol (500 µM) was directly added to the medium. Cells were further incubated at 37°C under 5% CO_2 for 30 min and then treated with H_2O_2 (at a final concentration of 1 mM) for 1 min. The reaction was quenched using a quencher solution containing 10 mM sodium ascorbate, 10 mM sodium azide and 5 mM Trolox. Cells were subsequently processed for immunostaining or immunoprecipitation.

Immunoprecipitation of biotinylated proteins

After biotin labeling, cells were scrapped using denaturing lysis buffer (1% SDS, 50 mM Tris-HCl pH 7.4 and 5 mM EDTA) containing 1× protease inhibitor cocktail (Complete Mini, Roche) at room temperature to completely denature the proteins. Afterwards, modified non-denaturing buffer (0.2% NP40, 50 mM Tris-HCl pH 7.4, 137 mM NaCl and 5 mM EDTA) was added to the lysed samples to dilute the SDS concentration to 0.1%. Subsequently, experimental groups were sonicated, and the protein concentration was measured using the Bradford method. Biotinylated proteins were then pulled down using streptavidin-coated magnetic beads. Beads were subsequently washed six times with RIPA lysis buffer (0.8% NP40, 50 mM Tris-HCl pH 7.4, 137 mM NaCl, 0.1% SDS and 5 mM EDTA), twice with 1× PBS and transferred to new tubes. One-tenth of the beads were retained for checking via western blotting.

Trypsin digestion for 6-plex TMT labeling

Biotinylated proteins from the EBSS and His groups were immunoprecipitated using streptavidin-coated magnetic beads. The immunoprecipitates were eluted using 80% trifluoroethanol (TFE)/0.1% trifluoroacetic acid (TFA) and dried in a Speed-Vac. Dried samples were dissolved in 250 mM triethylammonium bicarbonate (TEABC), reduced with 5 mM tris(2-carboxyethyl)phosphine (TCEP) at 60°C for 1 h, alkylated with 10 mM methyl methanethiosulfonate (MMTS) for 30 min at room temperature and digested with sequencing grade modified porcine trypsin (20 µg/ml) (Promega, Madison, WI) overnight at 37°C. Tryptic digested peptides were dried in a Speed-Vac, dissolved in 100 mM TEABC and subjected to TMT labeling according to the manufacturer's instruction (Thermo-Fisher Scientific). Labeled peptides were mixed and further desalted for 2D LC-MS/MS analysis.

2D LC-MS/MS analysis and database search for the TMT experiment

The peptide mixture was separated and analyzed by 2DLC-MS/MS using a strong cation exchange (SCX) and reverse-phase C18 liquid chromatography system on a Dionex UltiMate 3000 nano LC system coupled to a Orbitrap Fusion™ Lumos™ Tribrid™ Mass Spectrometer (Thermo-Fisher Scientific). The peptide mixture was reconstituted in HPLC buffer A (30% ACN and 0.1% FA) and loaded onto a homemade column (Luna SCX, bead size, 5 µm; column dimensions, 200×0.254 mm) (Phenomenex Inc., Torrance, CA) at flow rate of 2.5 µl/min for 20 min. The peptides were then fractionated into 26 fractions, using a continuous HPLC buffer B gradient (0–100% of 1 M ammonium nitrate in the presence of 25% ACN and 0.1% FA). Each fraction was then mixed with a stream of 0.1% FA in H_2O, and the peptides were trapped on a Zorbax C18 column (bead size, 5 µm; pore size, 30 nm; column dimensions, 5×0.3 mm) (Agilent Technologies Inc., Santa Clara, CA) and separated on a 60-min linear gradient of 99.9% ACN and 0.1% FA on a Hydro RP chromatography column (bead size, 2.5 µm; pore size, 10 nm; column dimensions, 200×0.075 mm) (Phenomenex Inc.). MS/MS analysis was performed on a Orbitrap Fusion Lumos mass spectrometer. Five full-scan MS ranges, including *m*/*z* 420–566, 562–652, 648–734, 730–844 and 840–1500, were acquired on the mass analyzer at a resolution of 60,000 at *m*/*z* 200, followed by MS/MS of the eight most-intense precursor ions using high-energy collision dissociation (HCD). Masses selected for MS/MS were isolated at a width of 0.7 *m*/*z* and fragmented with a normalized collision energy setting of 35%. The dynamic exclusion function was set as: repeat count, 1, and exclusion duration, 40 s. Proteome Discoverer (version 2.2, Thermo Fisher Scientific) was used to analyze the MS and MS/MS data. The Swiss-Prot database containing 20,259 entries for *Homo sapiens* (downloaded in March 2018) was used for identifying the proteins. Parent and fragment ion mass tolerance were set to 10 ppm and 0.03 Da, respectively. Two missed cleavages were allowed for tryptic digestion. For protein identification, oxidation of methionine, protein N-terminal acetylation and pyro-glutamination for N-terminal glutamine were set as variable modifications, whereas methylthiolation of cysteine was set as a fixed modification. Additionally, TMT labeling of lysine and the N-termini of peptides was added. Peptide identification criteria were set as: peptide confidence, high; minimum peptide length, 6; and FDR <0.01. In total, 3404 high confidence proteins containing at least two unique peptides were quantified. The median ratio of the quantified proteins between the experimental group (His) and control group (EBSS) in triplicate and corresponding *P*-value were calculated (Table S2). We set the cutoff at mean+2 s.d. and *P*-value ≤0.05 for selecting candidate proteins that might be significant interacting proteins of CTPS filaments.

Gene ontology analysis

Proteins identified in TMT labeling assay were used for Gene Ontology analysis. GSEA for biological process was performed using GESA_4.0.1 software utilizing MSigDB version 7.0 (Table S3) (Mootha et al., 2003; Subramanian et al., 2005).

Western blot analysis

For routine protein detection using western blotting, cells were lysed using ice-cold RIPA lysis buffer (50 mM Tris-HCl pH 7.4, 150 mM NaCl, 0.1% SDS, 1% TritonX-100 and 5 mM EDTA) containing 1× protease inhibitor on ice for 30 min. Samples were sonicated, and the protein concentration was measured before running SDS-PAGE. Proteins were transferred from SDS-PAGE gels to PVDF membranes and then blocked with blocking buffer [7% nonfat milk in Tris-buffered saline with 0.1% Tween 20 (TBST)] for 1 h. Afterwards, membranes were incubated overnight with primary antibody in blocking buffer at 4°C and then washed thrice with TBST for 5, 10 and 15 min. Membranes were then incubated with secondary antibody in blocking buffer at room temperature and subsequently washed thrice in TBST before development using ECL Pro.

Measurement of labeled UTP and CTP

A total of 8×10^5 cells were transfected with SNAP29 and scrambled siRNA using Lipofectamine 2000 (Thermo Fisher Scientific, cat. no. 11668019). The siRNA sequence for SNAP29 was 5′-AGACAGAAAUUGAGGAGCA-3′. At 24 h post transfection, cells were re-seeded into three groups (DMEM, EBSS and EBSS+His). SNAP29 knockdown was confirmed using western blotting, and simultaneous immunostaining with anti-CTPS antibody was performed to reconfirm that SNAP29 knockdown cells had reduced CTPS filaments in EBSS+His (200 µM) at 6 h. For UTP and CTP measurement, cells were incubated with $^{13}C^{15}N$-uridine (100 µM) for 1 h before harvesting with methanol. Supernatants were further dried and re-suspended in 2 mM dibutylamine and 1.5 mM formic acid. Cell extracts were analyzed by LC-MS (LTQ-orbitrap, Thermo). Details of the method were previously described in Lin et al. (2018). For the overexpression experiment, a total of 5×10^5 cells were transfected with SNAP29 and scrambled siRNA during seeding. At 16 h post transfection, cells were again transfected with WT-SNAP29 and siRNA-resistant SNAP29 constructs. After 24 h, cells were subjected to EBSS+His condition for 5 h followed by treatment with $^{13}C^{15}N$-uridine (100 µM) for 1 h in the same medium.

PLA

A total of 6×10^4 HEp-2 cells were seeded for PLA experiments. After fixation (4% formaldehyde and 4% sucrose in 1× PBS) and permeabilization (100% ice-cold methanol), PLA (Duolink PLA, DUO92101 Sigma) was performed based on the manufacturer's protocol.

Immunogold labeling and TEM

Transfected cells were pre-fixed in 2% paraformaldehyde and 1.25% glutaraldehyde followed by post-fixation in 1% osmium tetroxide solution for 1 h (EMS Microscopy Academy). After dehydration in a graded series of ethanol, cell pellets were embedded by Spurr's resin and then polymerized in an oven at 70°C for 8 h. Ultrathin sections (70 nm) were cut using a Leica UC7 ultramicrotome and collected onto a nickel grid for further immunogold labeling. These sections were first treated with 10% H_2O_2 for 10 min, followed by 1% BSA to block non-specific binding. Subsequently, samples were incubated with an anti-Flag antibody (Sigma-Aldrich, cat.no. F3165) for 1 h. The 18-nm immunogold-conjugated antibody (Abcam) was used to detect the Flag-tagged protein. Finally, the sections were post-stained with 4% uranyl acetate for 10 min and rinsed several times with H_2O followed by 4% Reynolds lead citrate for 10 min. Micrographs were obtained at 100 kV in a JEM-1230 transmission electron microscopy (JEOL) with a Gatan Model 832 digital camera.

DAB staining of target structures by APEX2

Cells transfected with FLAG–CTPS1–APEX2 or KRT18–APEX2 were incubated in EBSS+His (200 µM) or DMEM for 4 h. The protocol for DAB staining from a previous study was followed (Martell et al., 2017). The transfected cells were fixed in 2% glutaraldehyde followed by 0.5 mg/ml 3,3-diaminobenzidine (DAB) staining with 10 mM H_2O_2. Osmium tetroxide (1%) was used for post-fixation at 4°C for 30 min. Further dehydration and resin embedding were processed by standard EM sample preparation. Ultrathin sections (70 nm) were obtained by a Leica UC7 ultramicrotome. Uranyl acetate and Reynolds lead citrate (both at 4%) were used for negative staining of sections.

Immunoprecipitation of KRT8

A total of 2×10^6 cells were seeded overnight in 10-cm plates before replacing with conditional medium (EBSS+His) for 2 h. NEM at 1 mM was added to one of the plates for 10 min, and subsequently cells were scratched with KRT lysis buffer (20 mM Tris-HCl pH 7.4, 137 mM NaCl, 10% glycerol, 0.5% Triton X-100, 2 mM EDTA, 1× protease inhibitor cocktail, 1× phosphatase inhibitor cocktail) on ice. After 30 min of incubation on ice, lysed cells were sonicated and spun down at 15,000 ***g*** for 15 min to collect the supernatant. Protein A agarose beads (20 µl; Millipore 16-125) were added to each sample and incubated for 1 h at 4°C on a rotor for the pre-clearing assay. Samples were then spun at 13,200 ***g*** for 5 min to collect the supernatant. Next, the protein concentration was measured, and equal amounts of protein were used for the immunoprecipitation assay. Samples were rotated at 4°C overnight with anti-KRT8 antibody (Proteintech, cat.no. 10384-1-AP). Subsequently, samples were incubated with protein A beads for 1 h and then washed with KRT lysis buffer five times (1 min each). Beads were washed twice with 1× PBS and transferred to a new tube and further boiled with 2× SDS sample buffer.

Fluorescence microscopy and live cell imaging

Confocal images were acquired using a Zeiss Laser Scanning Confocal Microscope (LSM) 780 using Plan-Apochromat 100×1.40 Oil DIC M27 and Plan-Apochromat 20×/0.8 M27 lenses. For super-resolution images, ELYRA PS.1 super-resolution microscopy was used (Imaging Core, Academia Sinica, Taiwan). For live-cell imaging, images were acquired on a DeltaVision Ultra microscope (GE Healthcare) using a 60×1.42NA PlanApo N objective (Olympus) and an sCMOS camera; on a Nikon Ti2 Dragonfly High Speed confocal platform using a Nikon 100×/1.49 oil objective; and on LSM 780 confocal microscope using an Alpha Plan-Apochromat 100×/1.40 oil DIC M27 objective. Images and videos were processed using Fiji (ImageJ) (Schindelin et al., 2012) and Imaris (Bitplane).

Quantification and statistical analysis

For experimental data, a Student's two-tailed unpaired *t*-test was used for the analysis. Figure legends include all statistical details of the experiments.

Acknowledgements

We thank the Proteomics Core Laboratory at Chang Gung University for assistance with proteomic analysis. We thank the Imaging Core at Academia Sinica and Chang Gung University for assistance in super-resolution, live-cell and confocal imaging. We thank Sue-Ping Lee at Academia Sinica for helping us with super-resolution imaging. We thank the National RNAi Core Facility at Academia Sinica for providing shRNA reagents and related services. We thank FlyBase for providing information regarding the SNAP29 *Drosophila* gene. We thank Bloomington Stock Center and Fly Core Taiwan for providing fly stocks. We are grateful to the comments from Drs Mark Peifer, Robert Duronio, Laura Nilson, Juli Wu and Joerg Grosshans, Chien-Kuo Lee on the manuscript.

Competing interests

The authors declare no competing or financial interests.

Author contributions

Conceptualization: A.C., L.-M.P.; Methodology: A.C., L.-M.P.; Validation: A.C., W.-C.L., K.-Y.C., L.-M.P.; Formal analysis: A.C., Y.-T.L., I.Y.-F.C., H.-I.W.; Investigation: A.C., W.-C.L., Y.-T.L., K.-J.H., P.-Y.W., K.-T.M., C-.Y.W., X.-R.H., Y.-H.L., B.-C.C., Y.-J.H.; Resources: K.-Y.C., T-Y.L., J.-L.L., L.-Y.S., J.-S.Y., Y.-S.C.; Data curation: A.C., Y.-T.L., J.-S.Y., L.-M.P.; Writing - original draft: A.C., L.-M.P.; Writing - review & editing: L.-M.P.; Visualization: A.C., L.-M.P.; Supervision: Y.-S.C., L.-M.P.; Project administration: L.-M.P.; Funding acquisition: W.-C.L., J.-S.Y., L.-M.P.

Funding

This study was funded by the Ministry of Science and Technology, Taiwan (MOST 108-2311-B-182-004-MY3 to L.-M.P. and MOST 108-2321-B-182-004-MY3 to W.-C.L.); the Chang Gung Memorial Hospital, Linkou, Taiwan (CMRPD1H0191 to L.-M.P.); and the Molecular Medicine Research Center, Chang Gung University from The Featured Areas Research Center Program within the framework of the Higher Education Sprout Project by the Ministry of Education (MOE).

Data availability

The mass spectrometry proteomics data for iTRAQ labeling and TMT labeling have been deposited with the ProteomeXchange Consortium via the PRIDE (Vizcaíno et al., 2016) partner repository with the dataset identifiers PXD010921 and PXD015507, respectively.

Supplementary information

Supplementary information available online at
http://jcs.biologists.org/lookup/doi/10.1242/jcs.240200.supplemental

Peer review history

The peer review history is available online at
https://jcs.biologists.org/lookup/doi/10.1242/jcs.240200.reviewer-comments.pdf

References

Abada, A., Levin-Zaidman, S., Porat, Z., Dadosh, T. and Elazar, Z. (2017). SNARE priming is essential for maturation of autophagosomes but not for their formation. *Proc. Natl. Acad. Sci. USA* **114**, 12749-12754. doi:10.1073/pnas.1705572114

An, S., Kumar, R., Sheets, E. D. and Benkovic, S. J. (2008). Reversible compartmentalization of de novo purine biosynthetic complexes in living cells. *Science* **320**, 103-106. doi:10.1126/science.1152241

Anderson, P. and Kedersha, N. (2008). Stress granules: the Tao of RNA triage. *Trends Biochem. Sci.* **33**, 141-150. doi:10.1016/j.tibs.2007.12.003

Aughey, G. N., Grice, S. J., Shen, Q.-J., Xu, Y., Chang, C.-C., Azzam, G., Wang, P.-Y., Freeman-Mills, L., Pai, L.-M., Sung, L.-Y. et al. (2014). Nucleotide synthesis is regulated by cytoophidium formation during neurodevelopment and adaptive metabolism. *Biol. Open* **3**, 1045-1056. doi:10.1242/bio.201410165

Aughey, G. N., Grice, S. J. and Liu, J. L. (2016). The Interplay between Myc and CTP Synthase in Drosophila. *PLoS Genet.* **12**, e1005867. doi:10.1371/journal.pgen.1005867

Baek, A., Yoon, S., Kim, J., Baek, Y. M., Park, H., Lim, D., Chung, H. and Kim, D. E. (2017). Autophagy and KRT8/keratin 8 protect degeneration of retinal pigment epithelium under oxidative stress. *Autophagy* **13**, 248-263. doi:10.1080/15548627.2016.1256932

Barry, R. M., Bitbol, A. F., Lorestani, A., Charles, E. J., Habrian, C. H., Hansen, J. M., Li, H. J., Baldwin, E. P., Wingreen, N. S., Kollman, J. M. et al. (2014).

Large-scale filament formation inhibits the activity of CTP synthetase. *Elife* **3**, e03638. doi:10.7554/eLife.03638.036

Boeynaems, S., Alberti, S., Fawzi, N. L., Mittag, T., Polymenidou, M., Rousseau, F., Schymkowitz, J., Shorter, J., Wolozin, B., Van Den Bosch, L. et al. (2018). Protein phase separation: a new phase in cell biology. *Trends Cell Biol.* **28**, 420-435. doi:10.1016/j.tcb.2018.02.004

Buchan, J. R. (2014). mRNP granules. Assembly, function, and connections with disease. *RNA Biol.* **11**, 1019-1030. doi:10.4161/15476286.2014.972208

Calise, S. J., Carcamo, W. C., Krueger, C., Yin, J. D., Purich, D. L. and Chan, E. K. (2014). Glutamine deprivation initiates reversible assembly of mammalian rods and rings. *Cell. Mol. Life Sci.* **71**, 2963-2973. doi:10.1007/s00018-014-1567-6

Carcamo, W. C., Satoh, M., Kasahara, H., Terada, N., Hamazaki, T., Chan, J. Y., Yao, B., Tamayo, S., Covini, G., von Muhlen, C. A. et al. (2011). Induction of cytoplasmic rods and rings structures by inhibition of the CTP and GTP synthetic pathway in mammalian cells. *PLoS ONE* **6**, e29690. doi:10.1371/journal.pone.0029690

Chang, C. C., Keppeke, G. D., Sung, L. Y. and Liu, J. L. (2018). Interfilament interaction between IMPDH and CTPS cytoophidia. *FEBS J.* **285**, 3753-3768. doi:10.1111/febs.14624

Chen, K., Zhang, J., Tastan, Ö. Y., Deussen, Z. A., Siswick, M. Y.-Y. and Liu, J.-L. (2011). Glutamine analogs promote cytoophidium assembly in human and Drosophila cells. *J. Genet. Genomics* **38**, 391-402. doi:10.1016/j.jgg.2011.08.004

Endrizzi, J. A., Kim, H., Anderson, P. M. and Baldwin, E. P. (2004). Crystal structure of Escherichia coli cytidine triphosphate synthetase, a nucleotide-regulated glutamine amidotransferase/ATP-dependent amidoligase fusion protein and homologue of anticancer and antiparasitic drug targets. *Biochemistry* **43**, 6447-6463. doi:10.1021/bi0496945

Fuchs-Telem, D., Stewart, H., Rapaport, D., Nousbeck, J., Gat, A., Gini, M., Lugassy, Y., Emmert, S., Eckl, K., Hennies, H. C. et al. (2011). CEDNIK syndrome results from loss-of-function mutations in SNAP29. *Br. J. Dermatol.* **164**, 610-616. doi:10.1111/j.1365-2133.2010.10133.x

Glick, B. S. and Rothman, J. E. (1987). Possible role for fatty acyl-coenzyme A in intracellular protein transport. *Nature* **326**, 309-312. doi:10.1038/326309a0

Goto, M., Omi, R., Nakagawa, N., Miyahara, I. and Hirotsu, K. (2004). Crystal structures of CTP synthetase reveal ATP, UTP, and glutamine binding sites. *Structure* **12**, 1413-1423. doi:10.1016/j.str.2004.05.013

Gou, K.-M., Chang, C.-C., Shen, Q.-J., Sung, L.-Y. and Liu, J.-L. (2014). CTP synthase forms cytoophidia in the cytoplasm and nucleus. *Exp. Cell Res.* **323**, 242-253. doi:10.1016/j.yexcr.2014.01.029

Guo, B., Liang, Q., Li, L., Hu, Z., Wu, F., Zhang, P., Ma, Y., Zhao, B., Kovacs, A. L., Zhang, Z. et al. (2014). O-GlcNAc-modification of SNAP-29 regulates autophagosome maturation. *Nat. Cell Biol.* **16**, 1215-1226. doi:10.1038/ncb3066

Huang, Y., Wang, J.-J., Ghosh, S. and Liu, J.-L. (2017). Critical roles of CTP synthase N-terminal in cytoophidium assembly. *Exp. Cell Res.* **354**, 122-133. doi:10.1016/j.yexcr.2017.03.042

Ingerson-Mahar, M., Briegel, A., Werner, J. N., Jensen, G. J. and Gitai, Z. (2010). The metabolic enzyme CTP synthase forms cytoskeletal filaments. *Nat. Cell Biol.* **12**, 739-746. doi:10.1038/ncb2087

Kursula, P., Flodin, S., Ehn, M., Hammarström, M., Schüler, H., Nordlund, P. and Stenmark, P. (2006). Structure of the synthetase domain of human CTP synthetase, a target for anticancer therapy. *Acta Crystallogr. Sect. F Struct. Biol. Cryst. Commun.* **62**, 613-617. doi:10.1107/S1744309106018136

Lam, S. S., Martell, J. D., Kamer, K. J., Deerinck, T. J., Ellisman, M. H., Mootha, V. K. and Ting, A. Y. (2015). Directed evolution of APEX2 for electron microscopy and proximity labeling. *Nat. Methods* **12**, 51-54. doi:10.1038/nmeth.3179

Lin, Y., Mori, E., Kato, M., Xiang, S., Wu, L., Kwon, I. and McKnight, S. L. (2016). Toxic PR poly-dipeptides encoded by the C9orf72 repeat expansion target LC domain polymers. *Cell* **167**, 789-802.e12. doi:10.1016/j.cell.2016.10.003

Lin, W.-C., Chakraborty, A., Huang, S.-C., Wang, P.-Y., Hsieh, Y.-J., Chien, K.-Y., Lee, Y.-H., Chang, C.-C., Tang, H.-Y., Lin, Y.-T. et al. (2018). Histidine-dependent protein methylation is required for compartmentalization of CTP synthase. *Cell Reports* **24**, 2733-2745.e2737. doi:10.1016/j.celrep.2018.08.007

Liu, J.-L. (2010). Intracellular compartmentation of CTP synthase in Drosophila. *J. Genet. Genomics* **37**, 281-296. doi:10.1016/S1673-8527(09)60046-1

Loschke, F., Seltmann, K., Bouameur, J. E. and Magin, T. M. (2015). Regulation of keratin network organization. *Curr. Opin. Cell Biol.* **32**, 56-64. doi:10.1016/j.ceb.2014.12.006

Lynch, E. M., Hicks, D. R., Shepherd, M., Endrizzi, J. A., Maker, A., Hansen, J. M., Barry, R. M., Gitai, Z., Baldwin, E. P. and Kollman, J. M. (2017). Human CTP synthase filament structure reveals the active enzyme conformation. *Nat. Struct. Mol. Biol.* **24**, 507-514. doi:10.1038/nsmb.3407

Margiotta, A. and Bucci, C. (2016). Role of intermediate filaments in vesicular traffic. *Cells* **5**, E20. doi:10.3390/cells5020020

Martell, J. D., Deerinck, T. J., Sancak, Y., Poulos, T. L., Mootha, V. K., Sosinsky, G. E., Ellisman, M. H. and Ting, A. Y. (2012). Engineered ascorbate peroxidase as a genetically encoded reporter for electron microscopy. *Nat. Biotechnol.* **30**, 1143-1148. doi:10.1038/nbt.2375

Martell, J. D., Deerinck, T. J., Lam, S. S., Ellisman, M. H. and Ting, A. Y. (2017). Electron microscopy using the genetically encoded APEX2 tag in cultured mammalian cells. *Nat. Protoc.* **12**, 1792-1816. doi:10.1038/nprot.2017.065

Maruthappu, T., Chikh, A., Fell, B., Delaney, P. J., Brooke, M. A., Levet, C., Moncada-Pazos, A., Ishida-Yamamoto, A., Blaydon, D., Waseem, A. et al. (2017). Rhomboid family member 2 regulates cytoskeletal stress-associated Keratin 16. *Nat. Commun.* **8**, 14174. doi:10.1038/ncomms14174

Mastrodonato, V., Morelli, E. and Vaccari, T. (2018). How to use a multipurpose SNARE: the emerging role of Snap29 in cellular health. *Cell Stress* **2**, 72-81. doi:10.15698/cst2018.04.130

Mitrea, D. M. and Kriwacki, R. W. (2016). Phase separation in biology; functional organization of a higher order. *Cell Commun. Signal.* **14**, 1. doi:10.1186/s12964-015-0125-7

Mootha, V. K., Lindgren, C. M., Eriksson, K. F., Subramanian, A., Sihag, S., Lehar, J., Puigserver, P., Carlsson, E., Ridderstrale, M., Laurila, E. et al. (2003). PGC-1α-responsive genes involved in oxidative phosphorylation are coordinately downregulated in human diabetes. *Nat. Genet.* **34**, 267-273. doi:10.1038/ng1180

Morelli, E., Ginefra, P., Mastrodonato, V., Beznoussenko, G. V., Rusten, T. E., Bilder, D., Stenmark, H., Mironov, A. A. and Vaccari, T. (2014). Multiple functions of the SNARE protein Snap29 in autophagy, endocytic, and exocytic trafficking during epithelial formation in Drosophila. *Autophagy* **10**, 2251-2268. doi:10.4161/15548627.2014.981913

Noree, C., Sato, B. K., Broyer, R. M. and Wilhelm, J. E. (2010). Identification of novel filament-forming proteins in Saccharomyces cerevisiae and Drosophila melanogaster. *J. Cell Biol.* **190**, 541-551. doi:10.1083/jcb.201003001

Noree, C., Monfort, E., Shiau, A. K. and Wilhelm, J. E. (2014). Common regulatory control of CTP synthase enzyme activity and filament formation. *Mol. Biol. Cell* **25**, 2282-2290. doi:10.1091/mbc.e14-04-0912

Ostrander, D. B., O'Brien, D. J., Gorman, J. A. and Carman, G. M. (1998). Effect of CTP synthetase regulation by CTP on phospholipid synthesis in Saccharomyces cerevisiae. *J. Biol. Chem.* **273**, 18992-19001. doi:10.1074/jbc.273.30.18992

Pai, L.-M., Wang, P.-Y., Lin, W.-C., Chakraborty, A., Yeh, C.-T. and Lin, Y.-H. (2016). Ubiquitination and filamentous structure of cytidine triphosphate synthase. *Fly (Austin)* **10**, 108-114. doi:10.1080/19336934.2016.1182268

Petrovska, I., Nuske, E., Munder, M. C., Kulasegaran, G., Malinovska, L., Kroschwald, S., Richter, D., Fahmy, K., Gibson, K., Verbavatz, J. M. (2014). Filament formation by metabolic enzymes is a specific adaptation to an advanced state of cellular starvation. *Elife* **3**, e02409. doi:10.7554/eLife.02409.036

Rapaport, D., Lugassy, Y., Sprecher, E. and Horowitz, M. (2010). Loss of SNAP29 impairs endocytic recycling and cell motility. *PLoS ONE* **5**, e9759. doi:10.1371/journal.pone.0009759

Schindelin, J., Arganda-Carreras, I., Frise, E., Kaynig, V., Longair, M., Pietzsch, T., Preibisch, S., Rueden, C., Saalfeld, S., Schmid, B. et al. (2012). Fiji: an open-source platform for biological-image analysis. *Nat. Methods* **9**, 676-682. doi:10.1038/nmeth.2019

Shen, Q.-J., Kassim, H., Huang, Y., Li, H., Zhang, J., Li, G., Wang, P. Y., Yan, J., Ye, F. and Liu, J. L. (2016). Filamentation of metabolic enzymes in saccharomyces cerevisiae. *J. Genet. Genomics* **43**, 393-404. doi:10.1016/j.jgg.2016.03.008

Snider, N. T. and Omary, M. B. (2014). Post-translational modifications of intermediate filament proteins: mechanisms and functions. *Nat. Rev. Mol. Cell Biol.* **15**, 163-177. doi:10.1038/nrm3753

Sprecher, E., Ishida-Yamamoto, A., Mizrahi-Koren, M., Rapaport, D., Goldsher, D., Indelman, M., Topaz, O., Chefetz, I., Keren, H., O'Brien, J. T. et al. (2005). A mutation in SNAP29, coding for a SNARE protein involved in intracellular trafficking, causes a novel neurocutaneous syndrome characterized by cerebral dysgenesis, neuropathy, ichthyosis, and palmoplantar keratoderma. *Am. J. Hum. Genet.* **77**, 242-251. doi:10.1086/432556

Steegmaier, M., Yang, B., Yoo, J.-S., Huang, B., Shen, M., Yu, S., Luo, Y. and Scheller, R. H. (1998). Three novel proteins of the syntaxin/SNAP-25 family. *J. Biol. Chem.* **273**, 34171-34179. doi:10.1074/jbc.273.51.34171

Strochlic, T. I., Stavrides, K. P., Thomas, S. V., Nicolas, E., O'Reilly, A. M. and Peterson, J. R. (2014). Ack kinase regulates CTP synthase filaments during Drosophila oogenesis. *EMBO Rep.* **15**, 1184-1191. doi:10.15252/embr.201438688

Subramanian, A., Tamayo, P., Mootha, V. K., Mukherjee, S., Ebert, B. L., Gillette, M. A., Paulovich, A., Pomeroy, S. L., Golub, T. R., Lander, E. S. et al. (2005). Gene set enrichment analysis: a knowledge-based approach for interpreting genome-wide expression profiles. *Proc. Natl. Acad. Sci. USA* **102**, 15545-15550. doi:10.1073/pnas.0506580102

Uversky, V. N. (2017). Intrinsically disordered proteins in overcrowded milieu: Membrane-less organelles, phase separation, and intrinsic disorder. *Curr. Opin. Struct. Biol.* **44**, 18-30. doi:10.1016/j.sbi.2016.10.015

Vizcaíno, J. A., Csordas, A., del-Toro, N., Dianes, J. A., Griss, J., Lavidas, I., Mayer, G., Perez-Riverol, Y., Reisinger, F., Ternent, T. et al. (2016). 2016 update of the PRIDE database and its related tools. *Nucleic Acids Res.* **44**, D447-D456. doi:10.1093/nar/gkv1145

Wang, P.-Y., Lin, W.-C., Tsai, Y.-C., Cheng, M.-L., Lin, Y.-H., Tseng, S.-H., Chakraborty, A. and Pai, L.-M. (2015). Regulation of CTP synthase filament formation during DNA endoreplication in Drosophila. *Genetics* **201**, 1511-1523. doi:10.1534/genetics.115.180737

Weng, M. L. and Zalkin, H. (1987). Structural role for a conserved region in the CTP synthetase glutamine amide transfer domain. *J. Bacteriol.* **169**, 3023-3028. doi:10.1128/JB.169.7.3023-3028.1987

Wiese, S., Reidegeld, K. A., Meyer, H. E. and Warscheid, B. (2007). Protein labeling by iTRAQ: a new tool for quantitative mass spectrometry in proteome research. *Proteomics* **7**, 340-350. doi:10.1002/pmic.200600422

Windoffer, R., Beil, M., Magin, T. M. and Leube, R. E. (2011). Cytoskeleton in motion: the dynamics of keratin intermediate filaments in epithelia. *J. Cell Biol.* **194**, 669-678. doi:10.1083/jcb.201008095

Zacharias, D. A., Violin, J. D., Newton, A. C. and Tsien, R. Y. (2002). Partitioning of lipid-modified monomeric GFPs into membrane microdomains of live cells. *Science* **296**, 913-916. doi:10.1126/science.1068539